NASA Technical Memorandum 81237

Comparisons of AEROX Computer Program Predictions of Lift and Induced Drag with Flight-Test Data

John Axelson and Gary C. Hill

August 1981

National Aeronautics and
Space Administration

NASA Technical Memorandum 81237

Comparisons of AEROX Computer Program Predictions of Lift and Induced Drag with Flight-Test Data

John Axelson
Gary C. Hill, Ames Research Center, Moffett Field, California

NASA
National Aeronautics and
Space Administration

Ames Research Center
Moffett Field, California 94035

TABLE OF CONTENTS

NOTATION

AR	wing aspect ratio, b^2/S
b	wing span
C_D	drag coefficient
C_{D_o}	minimum drag coefficient
C_L	lift coefficient
C_{L_B}	finite-wing camber lift coefficient
$C_{L_{opt}}$	optimum lift coefficient at $(L/D)_{max}$
c_{ℓ_o}	two-dimensional airfoil theoretical camber
$\bar{c}$	wing mean aerodynamic chord
D	body diameter
d	exponent in induced drag equations
J	AEROX airfoil designator
L/D	lift to drag ratio
M	Mach number
ROC	leading-edge radius-to-chord ratio
S	wing area
XCD	chordwise location of the shock on wing upper surface as a fraction of chord length
z	AEROX flow zone designation

For plots where axis offsets are used:

$C_D = C_D' + \Delta C_D$, where C_D' is the plotted value, and ΔC_D is the tabulated offset.

α	angle of attack
γ	ratio of specific heats (1.4 for air)
Δ	increment

δ	tail deflection
Λ	angle of sweep
$\bar{\Lambda}$	effective angle of sweep $\bar{\Lambda} = \sin^{-1}(\sin \Lambda \cos \alpha)$
π	3.1416

Subscripts:

cam	cambered
i	induced
le	leading edge
max	maximum
min	minimum
o	symmetrical; minimum
sep	separation

COMPARISONS OF AEROX COMPUTER PROGRAM PREDICTIONS OF LIFT AND INDUCED DRAG WITH FLIGHT-TEST DATA

John Axelson*

and

Gary C. Hill

Ames Research Center

SUMMARY

The AEROX aerodynamic computer program provides accurate predictions of induced drag and trim drag for the full angle of attack range and for Mach numbers from 0.4 to 3.0. This capability is demonstrated by comparing flight-test data and AEROX predictions for 17 different tactical aircraft. Values of minimum (skin-friction, pressure, and zero-lift wave) drag coefficients and lift coefficient offset due to camber (when required) were input from the flight-test data to produce total lift and drag curves. Generally, the comparisons of trimmed lift-drag polars show excellent agreement between the AEROX predictions and the in-flight measurements. It is also shown that the program can account for wing leading-edge devices and induced effects of fuselage and engine nacelles, and that it can predict buffet onset as well.

INTRODUCTION

This study presents comparisons of known trimmed lift-drag polars, measured in flight for 17 military jet aircraft, with predictions from the AEROX aerodynamics computer program. The AEROX program was recently developed at Ames Research Center. Ten additional fighters used in this study are not included here because of their security classifications. AEROX methodology and the computer program were introduced and described in detail in reference 1; the program is validated through extensive comparisons with wind-tunnel data in the three volumes of reference 2. The AEROX program is available through the COSMIC program library (Program ARC 11,133; COSMIC; Barrow Hall, University of Georgia, Athens, Ga. 30601).

Because of the exceptionally rapid computer execution time (typified by 30 alpha Mach number sets of longitudinal aerodynamics per second on the IBM 360), AEROX is ideally suited for use in preliminary design and mission-optimization studies. The program calculates the coefficients of lift, drag due-to-lift, trim drag, and pitching-moment for aircraft and for their separate principal components to very high angles of attack (60°) for subsonic,

---

*Present address: 3054 Ebano Drive, Walnut Creek, California.

transonic, and supersonic speeds. Low-speed flows below M = 0.3, which are subject to dominant viscous effects and the estimation of minimum drag, are not calculated in AEROX. The minimum drag coefficients may be entered as an input and included in the total drag output, or the program can be coupled to another minimum drag routine such as that contained in the comprehensive CAPAIR assembly at Ames Research Center.

A review of the fundamental concepts used in AEROX is included to aid in the understanding of program options and outputs. The choice of appropriate airfoil designators and the possible inclusion of small camber offsets are shown to account for leading-edge devices and for anomalies in airfoil or wing geometry. The flow-zone designation included in the program output is shown to also provide a close estimate of buffet onset.

AEROX FUNDAMENTALS

The concepts and theories formulated in the AEROX computer program were described in detail in reference 2, which also serves as the users' guide to the COSMIC AEROX program (ARC 11,133); however, the basic precepts are reviewed here before the program estimates and flight data are compared. AEROX divides the flight envelope into six zones. Because the flow within each zone has unique characteristics, different sets of equations are required to determine lift and induced drag. The six flow zones and their boundaries are illustrated in figure 1(a). The location of the flow zone boundaries is dependent not only on Mach number and angle of attack, but also on the geometry of the aircraft.

The flow zones and boundaries established by AEROX for five well-known fighter aircraft are shown in figure 1(b), where lift coefficient has been substituted for the ordinate angle of attack, as it was used in figure 1(a). Subsonic cruise generally occurs in zone 2 where highest lift-to-drag ratios are found. Maneuvering flight tends to enter zone 3 because higher lift coefficients are required. The boundaries separating subsonic and supersonic leading edges (denoted "iv" in fig. 1(a)) are spread over Mach numbers from 1.1 to 2.0 because of the differences in the leading-edge sweep angles of the aircraft in figure 1(b). Only the F-104, which has a sharp leading-edge wing, enters zone 5, supersonic flow with attached leading-edge shock.

Limit Mach Number

The concept of the local-limit Mach number is the basis for the designation of the transonic-flow zones 3 and 4 and of the corresponding applicable lift and induced-drag equations. References 1 and 2 explain how the Laitone-limit Mach number is a criterion for the maximum static-pressure recovery behind a shock wave in transonic flow. When the local Mach number around the nose or on the surface of the wing reaches the unique value of 1.483, the boundaries shown in figure 1(a) as "ii" and "iii," respectively, are reached, and entry into the Mach-limited flow zones shown in figure 1(b) occurs. The

Mach-limited flows are characterized by regions in which the local Mach number does not exceed 1.483. These regions, which grow with further increase of flight Mach number or angle of attack, are also characterized by increased induced drag and reduced lift-curve slope.

The leading-edge radius-to-chord ratio, ROC, is an influential parameter in determining flow zone boundaries. ROC may be input into the program directly, or calculated within the AEROX program by specifying an airfoil designator, J. The following families of airfoils are covered:

J	Airfoil
1	Sharp leading edge, or an airfoil with a ridge or discontinuity near the nose
2	NACA 00XX and 230XX airfoils
3	NACA 6-series airfoils
4	Slab airfoil with leading-edge radius at least one-half the airfoil thickness
5	Default designator, used when ROC is input as a specified value

Another parameter that is important to AEROX is the chordwise location of the terminal shock, XCD. XCD is used only in zone 4, a flow regime reached only in high transonic maneuvering.

Further details on each of the flow zones follow.

Incompressible Flow Zone 1

This low-speed zone for Mach numbers below approximately 0.2 is used primarily for theoretical development of the equations to which compressibility factors are added. The aerodynamics in zone 1, especially at higher angles of attack, are subject to large viscous effects not amenable to simple analysis. Furthermore, the data of interest here are for higher Mach numbers. No further emphasis will be placed on zone 1.

Compressible, Shock-Free Flow Zone 2

Optimum subsonic cruise and maximum lift-drag ratios generally occur in zone 2. Flow zone 2 is illustrated in figures 2(a) and 2(b). The lift and induced drag are determined from traditional potential-flow equations with appropriate compressibility factors. A Prandtl-Glauert factor attenuated with increasing angle of attack is applied to the upper-surface lift, and a pitot compressibility factor is applied to the lower-surface lift. Only airfoils having rounded or blunted leading edges ($J > 1$) are treated with zone-2 equations; sharp leading-edge airfoils ($J = 1$) are treated in zones 3 to 6.

Designers of transonic aircraft usually strive to keep as much of the flight operations as possible in zone 2, where the lowest induced-drag and highest lift-drag ratios occur.

Leading-Edge Mach-Limited Flow Zone 3

The onset of the Laitone limit Mach number on the nose of the wing is related to the leading-edge radius-to-chord ratio, ROC, and to the Mach number, M, by the following equation (ref. 1):

$$\alpha_{z=3} = \frac{\sqrt{1.528 - 0.695\ M^2}}{M\left(1 + \sqrt{\frac{2}{ROC}}\right)}$$

Mach-limited flow is treated as nonpotential flow, and lift is calculated from momentum lift equations derived in references 1 and 2. Sharp airfoils or an airfoil having a prominent sharp ridge are also treated by the momentum equations. Examples of zone-3 flow are shown in figures 2(c) and 2(d). The use of leading-edge devices to gain camber or to delay the Mach limit or separation on the nose can incur the adversities of a sharp ridge line, as will be discussed later for specific aircraft examples. The use of the sharp airfoil designator, J = 1, for a blunt-nose airfoil with a sharp ridge will be shown to provide estimates in reasonable agreement with the data.

Surface Mach-Limited Flow Zone 4

Designation of this zone implies that the local-limit Mach number, 1.483, prevails along the wing upper surface to the designated chordwise location of the local normal shock (see fig. 2(e)). The onset of this zone is delayed to higher lift coefficients for more aft locations of the shock. The designation of the shock location, XCD, is not needed unless estimates are being made for zone 4. Most of the older aircraft with thrust-to-weight ratios well under unity cannot sustain steady flight in zone 4 because of the high induced drag. Separation drag is based on a flow model where the separation starts at the base of the local shock at the designated shock location:

$$C_{D_{sep}} = (b - D)(1 - XCD)\left(\frac{\bar{c} \sin \alpha}{2S}\right)$$

The chordwise shock location, XCD, may be determined from airfoil pressure distributions or flow visualizations when available, or a range of values may be entered in a parametric variation; a logical starting point is the chordwise location of maximum cross-sectional area. In this study, XCD was varied to best match the flight-test data. From the results of this analysis, a useful correlation of the shock location with either Mach number or with aspect ratio was made; it is presented in figure 3. This correlation provides the quickest choice of shock location. Figure 4 presents an algorithm for

estimating XCD that combines the effects of aspect ratio and flight Mach number. The equation

$$XCD = 1.0476AR^{-0.711}M^{0.405}$$

was derived from regression analysis using the XCD values that provided the closest fit to the flight-test data. The precision with which the XCD values are predicted is only 28%, as indicated by the scatter of the data points. However, considering the local flow disturbances occurring at points outside the design points, which are included here and discussed later, this relationship is sufficiently accurate for preliminary design work, when the aircraft is properly designed for the flight conditions. Note that most of the aircraft that were used to derive the data in figures 3 and 4 are newer and capable of the higher performance necessary to sustain flight in zone 4. As mentioned previously, these aircraft are not used in the comparisons presented here because their performance data are either classified or sensitive.

Supersonic Attached-Shock Zone 5

This flow zone, which is illustrated in figure 2(f), applies only to wings having sharp leading edges (J = 1), as used on the F-104 and B-70, and to angles of attack below that for shock detachment. The governing lift equations in AEROX are the momentum lift equation, with a Mach number attenuation for Mach numbers to 3, above which an explicit oblique-shock equation is used.

Supersonic Detached-Shock Zone 6

This flow zone, shown in figure 2(g), encompasses all blunt airfoils operating with supersonic leading edges, and all sharp airfoils operating at angles of attack above that for shock detachment. The momentum lift equation is used for the supersonic range, and a transition is made to incorporate modified Newtonian impact theory at hypersonic speeds.

Camber

Geometric camber results from curvature of the mean line of the basic airfoil, or from the deflection of leading-edge or trailing-edge flaps or, occasionally, from the shape of the aircraft fuselage, even though the airfoils are symmetric. In the cases of flap deflection, the chord line which passes through the flap nose (leading-edge flap) and through the flap trailing edge no longer coincides with the chord line of the basic airfoil with undeflected flaps. The original chord line for the basic airfoil is usually retained as reference for computing angle of attack, rather than the chord line of the deflected flap. The effects of the camber, whether from flaps or from curvature of the airfoil or body, are accounted for with the parameters C_{L_B} and $C_{D_{cam}}$, as shown in figure 5. The equations relating the symmetrical and cambered airfoils are based on the parabolic polars from classical elliptic wing theory; they apply to AEROX zone 2.

The theoretical camber effects of the two-dimensional airfoil section will not be realized in a finite-aspect-ratio wing. The actual camber-offset lift coefficient, C_{L_B}, is always less than the theoretical two-dimensional camber that is shown at the top of figure 6. The lower part of figure 6 shows the reduced actual camber-offset lift coefficient as sweep is introduced into the finite wing.

Since the reference axis for angle of attack is not changed from the basic airfoil chord line when leading-edge or trailing-edge flaps, nose droops, or slats are deflected, the actual camber offsets reflect both the camber effect and a shifted angle of attack for zero lift. Therefore, large leading-edge-device deflections may have small camber offsets. However, significant aerodynamic benefits can still result from aligning the nose of the airfoil to a lesser angle of attack, which changes the effective leading-edge radius and delays the onset of the leading-edge Mach limit flow. These effects will be illustrated by comparing conceptual lift-drag polars and lift curves for zones 2, 3, and 4.

Conceptual Transonic Lift and Drag Characteristics

Figure 7 illustrates conceptual lift and drag curves for zones 2, 3, and 4. In figure 7(a) the lift and drag curves are shown as they would be if the airfoil were being operated with the flow conditions described for these three zones over the range of angles of attack, without any transition between zones or crossing of the boundaries that were shown in figure 1(a). The best performance, as defined by the highest lift-to-drag ratios, is found in zone 2. The toll taken by Mach limit on or near the leading-edge is shown by the $z = 3$ line, and the further deterioration of performance for surface Mach limit by $z = 4$. Camber offsets are not appropriate for figure 7(a) because the changes in aerodynamic conditions between the zones are due to the onset and development of Mach-limited zones. For visualization of these flow zones review figure 2.

Figure 7(b) shows how lift and drag coefficients react when flow zones shift from 2 to 3 and then to zone 4, or shift directly from zone 2 to zone 4. In figure 1(b) we saw how the flow zone boundaries were dependent on the aircraft configuration. The effect of increased leading-edge radius or forward movement of the shock location, XCD, or both, is to displace the "ii" and "iii" boundaries vertically. Zone-3 type flow may not occur at all for some cases, resulting in a direct transition from zone 2 to 4. Flow zone boundaries correspond to the breaks on the curves of figure 7(b).

Buffet

The onset of zones 3 and 4 indicates that local Mach numbers are as high as 1.48. When these conditions have been reached, the accompanying shock waves, their possible oscillations due to instabilities, separation, and turbulence constitute the conditions indicative of buffet. The onset of the leading-edge Mach limit zone 3, designated as boundary "ii," is indicative of

the onset of light buffet. The transition line "iii" designating the presence of surface Mach-limited flow and accompanying separation provides an indication of heavy buffet. The onsets of buffet as observed or felt by the pilots in test flights of several aircraft are available in reference 3. The good agreement between the observed buffet boundaries and the onset of the leading-edge Mach zone 3 in AEROX is shown in figure 8. Interestingly, the same zone-3 boundaries estimated in AEROX were very close to the "design" lift coefficients cited in reference 3, which are designated as the maxima of the products of the Mach number and the corresponding maximum lift-drag ratio.

The flight-test data indicate that none of these aircraft had measured data in the surface Mach-limited flow conditions, zone 4, possibly because of insufficient thrust to maintain steady flight conditions necessary for measuring forces. It was not possible to correlate the onset of heavy buffet, nor was there any necessity of estimating the chordwise shock location XCD when comparing the measured flight-test data points with the AEROX estimates of lift and drag. It is only at higher lift coefficients, as measured in wind-tunnel tests or in more recent tests of higher thrust-to-weight aircraft capable of sustained high-g conditions, that the chordwise shock location for the correlation presented in figures 3 and 4 could be selected.

Equations for Induced-Drag Coefficients

Induced-drag coefficients are derived in AEROX by the following equations. Efficiency factors are not required, because the lift and drag of each component is calculated separately and summed for the total aircraft.

Zone	C_{D_i}
1, 2	$C_L^2/\pi AR$
3	$C_{L_{z=3}}^2/\pi AR + \Delta C_L(\tan\alpha)^d$
4	$C_{L_{z=4}}^2/\pi AR + \Delta C_L(\tan\alpha)^d + C_{D_{sep}}$
5, 6	$C_L \tan\alpha$

The lift coefficients with subscripts $z = 3$ or 4 are the transition values "ii" and "iii," respectively, in the curves of figure 7. The exponent d (DEXP in ref. 2) is assigned the following values:

$$M \leq 1 \qquad d = 1.5 - \frac{M}{4}\cos\bar{\Lambda}_{le}$$

$$M > 1 \qquad d = 1.5 - \frac{M^2}{4}\cos\bar{\Lambda}_{le}$$

The exponent is used to provide mathematical continuity through the zone transitions and provides compatibility between AEROX and optimizer programs by avoiding multivalue points.

Effects of Center-of-Gravity Location on Drag

To accurately estimate the trimmed lift-drag polars, careful attention must be given to the location of the center of gravity. In many reference reports these locations were not specified, or were not known accurately during the various phases of the flight test. To illustrate the effect of center-of-gravity location on the trimmed lift-drag polars, figure 9 shows the trimmed lift-drag curves for two different locations used in the flight tests of the F-5. These results demonstrate the importance of accounting for the longitudinal stability and the location of the center of gravity in any assessment of trimmed aircraft aerodynamics, especially at supersonic speeds.

Matching Predictions and Design Level

Tactical aircraft must comply with a diversity of performance specifications — for example, maximum speed, takeoff distance, landing-approach speeds, acceleration, turn rate, ceiling, heavy weapons loads, external carriage, and handling qualities — that can have opposing influences on the design. Emphasis on these requirements varies between aircraft types, their design missions, the weapons they may carry, and the threats they must oppose.

During initial or conceptual stages of aircraft design, only the gross or most influential design parameters are considered. The "simplistic" airplane usually is composed of candidate power plants, a fuselage to accommodate the internal payload, sufficient tail area, and a wing whose geometry is to be varied to achieve a "best" design. Airfoil section, leading-edge radius, wing incidence and sweep angles are usually assumed constant along the span. Such simplifications are convenient and often necessary when the large number of possible configurations involved in seeking the optimum for the diverse mission requirements are being assessed.

During the detailed design stage, attention is directed to such items as wing twist, cranked wings, dihedral, flap mechanism, gear and inlet locations, excrescences and stores carriage. To determine accurately the performance of these design refinements, wind-tunnel tests are used to augment the results from the estimating procedures.

Predictions of lift and drag using only the simplistic design inputs should not be expected to agree completely with in-flight measured characteristics. Indeed, the latter contain a significant margin of error, because of the limited accuracies and different data-reduction techniques involved. It will be demonstrated by several examples, however, that most anomalies in wing design and in the accompanying wing aerodynamics can still be well represented in the AEROX predictions through the choice of appropriate airfoil designator matched to the associated ranges of Mach number or angle of attack, and by the inclusion of a camber offset.

Until very recently, accurate in-flight measurements of drag and lift required unaccelerated constant-altitude flight. It has been common practice to adjust data from wind-tunnel tests to agree with the selected points from

in-flight tests to derive flight-test results over the full range of lift coefficients and Mach numbers. This is attested to by the number of flight-test lift-drag curves published for speeds and lift coefficients beyond the capabilities of the aircraft, and outside the region where steady-state flight can be maintained. This is not true for more modern fighters with their much greater thrust-to-weight ratios and improved techniques for taking drag measurements in flight, but it is the case for almost all the aircraft whose lift-drag curves are published herein.

AIRCRAFT DESCRIPTIONS

T-2 Buckeye

The T-2 Buckeye, illustrated in figure 10(a), is a basic trainer used by the Navy. Aerodynamic flight-test data for the T-2 are taken from reference 3 (see fig. 10(b)). This aircraft is used for jet transition through instrument flying and carrier indoctrination. The initial version (T-2A) was powered by a single turbojet engine. The T-2B used in this study is equipped with two J60 engines and is aerodynamically identical to the T-2C, which incorporates two J85 engines. The unswept wing is mid-mounted on the fuselage, which has a prominent tandem-cockpit canopy that accommodates a raised rear seat. The aircraft is also characterized by tip tanks and a wide-track main landing gear.

The T-2 wing is an NACA 64A212 airfoil, which is relatively thick (12% thickness-to-chord ratio) compared with the wings of the transonic and supersonic aircraft used in this study. High transonic speeds are not required for the training mission. The T-2's best cruise speed is about $M = 0.64$, $M(L/D)|_{max}$ occurs at $M = 0.723$, and maximum speed is limited to $M = 0.75$. The leading-edge radius of the NACA 64A212 airfoil is also relatively large; this delays the onset of the local-limit Mach number, zone 3, to beyond the limits of the measurable flight-test data.

T-37 Tweety Bird

The T-37 "Tweety Bird" is the primary jet trainer of the USAF (fig. 11(a)); its performance data (fig. 11(b)) are taken from reference 4. The T-37 has two J69 turbojet engines, which are installed in the wing root, and features side-by-side seating, giving the fuselage a tadpole profile.

The T-37 design speed is even lower than that of the T-2. The limiting speed on the airframe is $M = 0.7$, maximum aerodynamic efficiency $[M(L/D)|_{max}]$ is at $M = 0.675$, the top speed is $M = 0.6$, and best cruise or design speed is about $M = 0.46$ — truly a subsonic aircraft. The wing section of the T-37 varies from an NACA 2418 at the root to an NACA 2412 at the tip, a considerably higher thickness-to-chord ratio than will be exhibited by the other aircraft in our inventory. The leading-edge-to-chord ratio is also greater than for any of the others.

A-3 Skywarrior

The Navy A-3 Skywarrior (fig. 12(a)) is a three-place carrier- or land-based high-altitude bomber. Two J57 turbojet engines are installed on pylons in under-the-wing nacelles; all other aircraft in this study have internally mounted engines. The aerodynamic data (from ref. 5) are for the bomber version, the earliest and aerodynamically cleanest of many models built. More recent A-3's have been outfitted for electronic-counter-measures missions and air-to-air refueling tanker missions. Later models were also built with cambered airfoil sections for improved specific range, but only the uncambered wing is considered here.

The A-3 is designed for high-altitude cruise. Its maximum-range cruise speed is slightly above Mach 0.8, better than the other nonsupersonic tactical aircraft. Limit load factor is also about half that of other tactical and trainer aircraft, for it is a straight and level bomber without a requirement for high-g maneuvering. Maximum sustainable speed is Mach 0.885 at 35,000 ft.

The Skywarrior wing is equipped with "automatic" leading-edge slats. They are not driven by either hydraulic or electrical power; instead, they extend under their own weight and are retracted by aerodynamic forces. Reducing airspeed causes the slats to extend, as will increasing the g or vertical acceleration of the aircraft. Although the slats are low-speed devices, used to decrease landing and takeoff speeds, they do affect aircraft performance at the higher speeds and higher lift coefficients of concern in this study. Even though the slats do not extend at speeds above $M = 0.45$, this type of free-floating device is known to "unport" and cause a discontinuity in the smooth airfoil section at higher g loadings. This unporting is not a disadvantage for this aircraft, because the lift coefficients at which it occurs is above that for cruising flight, and there is no maneuverability design requirement.

A-4 Skyhawk

The Navy A-4 Skyhawk, a carrier-based, single-place, lightweight attack bomber, was in production for 25 years. The bifabricated inlet supplies air to a single J52 gas turbine engine. Older versions of the A-4 were powered by J65 engines. The aerodynamic data used in this report are from reference 6, which covers the A-4F version.

As can be seen in figure 13(a), the A-4 wing is a modified delta-planform, mounted low on the fuselage to allow a carry-through wing box structure. Keeping size and weight to a minimum was a primary design consideration on the A-4. The aspect ratio is much less for the A-4 than for any of the other subsonic designs considered, even less than many of the supersonic ones. This low aspect ratio eliminated the need for folding the A-4's wings aboard carriers, thus reducing the aircraft's weight.

The A-4 is equipped with "automatic" leading-edge slats, as is the A-3 (both were designed by the same company). No unporting problem was evidenced for the A-4, however, probably reflecting improved slat design.

RA-5 Vigilante

The A-5 Vigilante is a carrier-based, two-place, all-weather, supersonic combat aircraft. Originally designed as a supersonic strategic bomber, the A-5 has now become the RA-5 reconnaissance aircraft, the version used in this study; aerodynamic performance data on the RA-5 are from reference 7. The Vigilante is powered by twin afterburning J79 engines with variable geometry inlets, giving it a Mach 2.1 capability at altitude.

The clean lines of A-5 can be seen in figure 14(a). The wing has a very low thickness-to-chord ratio; it incorporates hydraulically operated variable-camber leading-edge devices to increase the subsonic cruise range. These are deployed 4.5° to improve cruise efficiency. The effect of these "cruise droops" is to create a camber offset and produce a decrease in the effective leading-edge radius-to-chord ratio. These same leading edge droops are retracted for supersonic flight and lowered 45° for landing and takeoff. Maximum aerodynamic efficiency occurs at $M = 0.896$, with the cruise droops deployed.

A-6 Intruder

The A-6 Intruder is a twin-engine, midwing monoplane with side-by-side seating for a crew of two (fig. 15(a)). This carrier-borne, low-level attack bomber can deliver a variety of conventional and nuclear weapons on targets completely obscured by weather or darkness. Powered by two J52, turbojet engines, the A-6 is characterized by a large radome, moderately swept-back wings, and a tadpole-shaped fuselage. A variety of A-6 models and derivatives have been operated by the U.S. Navy and Marine Corps.

The flight-test data for the aircraft (from ref. 8) indicate that the optimum aerodynamic speed $[M(L/D)|_{max}]$ is $M = 0.755$. The best specific range for the clean aircraft is achieved at $M = 0.75$. The low landing speed of the A-6, significantly slower than that of other tactical jet aircraft, is achieved by lower wing loading and by full span leading- and trailing-edge devices.

A small wing strake can be seen in the planform view of figure 15(a). This strake exerts considerable influence on the aerodynamics. The leading-edge of the strake is angled sharply, and the wing leading-edge radius-to-chord ratio is similar to that of other transonic aircraft. The A-6 has the highest ratio of maximum gross weight to empty weight of the attack aircraft considered. This means that high L/D's had to be maintained over a larger C_L range than for the others; this requirement may account for the use of the strake.

A-7 Corsair II

The A-7 Corsair II is a single-engine, single-place, subsonic, light-attack aircraft. The Navy A, B, and E versions are intended for carrier operations; the A-7D is used by the USAF and the Air National Guard. The A-7 is powered by a TF-30 (A, B) or TF-41 (D, E) non-afterburning turbofan engine, which gives it excellent range. Although the A-7 (fig. 16(a)) is notably similar to the F-8 Crusader, it is not a derivative of the F-8 design. The A-7 is shorter than the F-8 and the fineness ratio of the fuselage is considerably less, the aircraft not having been designed for supersonic flight. The A-7 also has a very large intake with a rounded lip, in contrast to the F-8's smaller, sharp-lip inlet.

The wings of the two aircraft are, however, almost identical in size and geometry, including the drooping of the leading edges to provide camber. The F-8 "cruise droops" reduce drag at subsonic cruise, and as on the RA-5 are retracted for supersonic flight where camber would increase drag. The forward 20% of the A-7 wing is permanently drooped 7°, cambering the otherwise NACA 65A007 airfoil section. A sharp break or ridge line is evident along that 20%-chord line of the upper surface of the wing. Ridge lines can increase induced drag by producing premature local Mach-limited flow. Although the intended benefits of the camber are realized, the ridge line can cause a deterioration in maneuvering performance at lift coefficients higher than those utilized in cruise. It is not known if the A-7 was designed to meet any sustained maneuver requirements in its original specifications.

F-4 Phantom II

The F-4 Phantom II is a two-place (tandem seating) supersonic long-range interceptor/fighter. It is powered by twin single-rotor, axial-flow, variable-stator J79 turbojet engines equipped with afterburners and vertical variable ramp inlets. The F-4 (fig. 17(a)) is recognizable by its low-mounted swept-back wings with dihedral at the tips and stabilator of considerable anhedral. The Phantom II is used by both the Navy and Air Force, and exported to many countries. Over 5,000 units of this very successful design have been built.

The F-4 is capable of level flight speed of near Mach 2.3, with maximum power and in the clean configuration, according to the flight-test data of reference 9, from which our performance data are taken. Maximum aerodynamic efficiency occurs at Mach 0.935, but the best range cruise is achieved at Mach 0.86. This illustrates one of the compromises that occur between the supersonic speed requirement and the desire for achieving high cruise efficiency.

F-5 Freedom Fighter

The F-5 Freedom Fighter is a high-performance, multipurpose, tactical fighter, which is produced in both single-place and two-place versions. F-5A aerodynamic data (ref. 10) are used in this study, but the variations in data

are slight, especially in the area of induced drag. As illustrated in figure 18(a), the fuselage is area-ruled, and the aircraft is exceptionally clean. The wing tips may be optionally configured with either tip tanks or missile launcher rails. Two afterburning J85 engines provide twin-engine reliability and supersonic flight capability.

The principal mission of visual air combat is accomplished with internally mounted guns and heat-seeking air-to-air missiles. It is also capable of delivering a variety of air-to-ground ordnance. The F-5 is designed to operate from unimproved fields, and has been used in many countries throughout the world. The design speed and maximum range cruise both occur at Mach 0.895. The maximum diving speed limitation is Mach 1.72, but maximum attainable speed for the F-5A straight and level is Mach 1.35. Maximum speeds and combat maneuverability are improved in later versions by more powerful engines and maneuver flaps.

F-8 Crusader

The F-8 Crusader is a single-place, carrier- or land-based supersonic fighter capable of combat at high altitudes. Dubbed "Mig Master" and "The Last of the Gun Fighters," the Crusader is the last fighter designed with guns as primary armament (it is now equipped to carry heat-seeking missiles). The aircraft was in production from 1955 to 1965. The F-8 (fig. 19(a)) is identified by the long slender fuselage with a sharp leading-edge intake mounted under the chin. The engine is a J79 with afterburning. Two dorsal fins are mounted vertically on the lower aft section of the fuselage and the horizontal tail moves as a unit to provide elevator control.

The thin, swept-back, two-position wing of the F-8 is mounted high on the fuselage. The variable incidence wing provides good pilot visability while the wing is operating at high angles of attack for takeoff and landing. The wing also incorporates full-span leading-edge droops and small trailing-edge flaps which lower 20° in conjunction with the ailerons (inboard of the wing fold) lowering 20° to further reduce approach speeds. "Dirty" configuration performance is not considered in this study, which is limited to cruise and maneuver performance.

The leading-edge droops may be deployed 7° for subsonic cruise to achieve a higher lift-to-drag ratio. With the droops deployed to the cruise position, the theoretic maximum cruise efficiency occurs at Mach 0.872. Maximum specific range is achieved at Mach 0.85, according to the aerodynamic data of reference 11. With the droops fully retracted to the clean configuration, the F-8C has a maximum speed of Mach 1.9.

F-11 Tiger

The F-11 Tiger, a lightweight fighter/interceptor, was the Navy's first supersonic fighter. Principal armament for the Tiger is four internally mounted guns and heat-seeking air-to-air missiles. The Tiger was used for several years by the Blue Angles, the Navy's aerobatic demonstration team.

It is single-placed and powered by an afterburning J65 engine. The fixed inlets are of bifurcated design. Aerodynamic performance of the F-11 is based on unpublished data, supplied by the manufacturer.

The cantilever wing of the F-11 is mid-mounted and mildly swept at 30° (fig. 20(a)). The wing is equipped with leading-edge slats, trailing-edge flaps, spoiler-type controls, and small trim tabs on the tips. The fuselage is waisted amidship, providing area-ruling for supersonic flight. Maximum sustained Mach number is 1.16. In the cleanest configuration, the best specific range occurs at $M = 0.87$ and the maximum aerodynamic efficiency at $M = 0.888$.

F-100 Super Sabre

The first of the USAF's "Century Series" fighters, the F-100 Super Sabre was the Free World's first aircraft capable of supersonic flight for extended periods of time. The F-100 has been built in both single- and tandem two-seat versions, and fulfills both tactical fighter and bomber roles. This aircraft was also used by the Thunderbirds, the USAF flight demonstration team. Data on the F-100 are from reference 12.

The Super Sabre is characterized by a nose inlet and low-mounted swept wing. A single afterburner-equipped J57 powers the F-100. The wing is equipped with automatic leading-edge slats, conventional trailing-edge flaps, and ailerons. The optimum cruise speed is about Mach 0.875; maximum sustainable speed is Mach 1.28. The three-view drawing of the F-100 in figure 21(a) shows a significant amount of camber of the fuselage; its effects were evidenced in the analysis. The previously discussed effects of unporting automatic leading-edge wing devices were also exhibited.

F-101 Voodoo

The F-101 Voodoo (fig. 22(a)) was designed as an escort fighter for long-range strategic bombers. However, it was never cast in that role, serving instead as an interceptor. Several variations of this high-performance aircraft were built, including a camera-ladened reconnaissance model and a tandem two-seater. The dual-cockpit models were most popular; they carried a radar fire control officer or an instructor pilot in the trainer models equipped with dual controls. The twin J57 engines with afterburners give the F-101 a high rate of climb for quick scramble and intercept missions. The inlets of this supersonic twin-jet fighter are in the wing roots; the tail is high mounted, almost a T-tail. A large straight-edge fillet on the inboard section of the wing trailing edge can be seen in the figure.

Based on the aerodynamic data of reference 13 the F-101 has a maximum M(L/D) at Mach 0.843. The maximum specific range is achieved at Mach 0.83. The variation of the higher "design speed" accommodates the supersonic maximum sustained speed of Mach 1.65. The airfoil section is given by reference 13 as NACA 65007 modified. The analysis showed that the modification likely includes some amount of camber.

F-104 Starfighter

During its career, the USAF's F-104 Starfighter has undergone a metamorphosis from a simple day-superiority fighter to a complex all-weather strike and reconnaissance aircraft with remarkably little visible change. Dubbed the "missile-with-a-man-in-it" the F-104 is characterized by its very small and thin wing with sharp leading edges. Boundary-layer control is incorporated into the wing trailing-edge flaps to reduce approach speed for landing. Another significant development on the F-104 is the half-cone inlets, which feed the single J79 engine. The horizontal stabilizer is a high-mounted T-tail, and a dorsal fin on the underside of the fuselage helps directional stability. An F-104C is illustrated in figure 23(a).

The F-104 can maintain a speed of Mach 2.2 at altitude. The maximum aerodynamic efficiency occurs at Mach 0.896 and specific range at Mach 0.87. The straight-edge wings are extremely thin and sharp, which contributes to the high-speed capabilities of this aircraft. The design is very straightforward, and shows little compromise for any requirements other than high speed. Data on F-104 are from reference 14.

F-105 Thunderchief

The F-105 Thunderchief was developed to meet USAF requirements for a supersonic fighter-bomber able to deliver nuclear weapons and heavy loads of conventional bombs and rockets at very high speeds and over long ranges. The fuselage, which has a large internal weapons bay, is wasp-waisted near the wing position. Unique forward-swept air intake ducts in the wing-root leading-edge provide a double shock wave to slow inlet air to the engine and reduce turbulence at the tail-plane. The engine is a single J75 afterburning turbojet, with water injection to augment takeoff performance. Either single-pilot or dual-tandem cockpits are provided. The single-seat aircraft is depicted in figure 24(a).

F-105 data are from reference 15. The mid-mounted wing is a conventional NACA 65 series airfoil, with leading- and trailing-edge devices as well as spoilers and ailerons for control. The full span leading-edge flaps may be deployed for improved subsonic cruise and maneuver. For the clean configuration, maximum cruise efficiency is achieved just below Mach 0.9; maximum speed is Mach 2.1.

F-106 Delta Dart

The USAF F-106 Delta Dart is a development version of the F-102. Extensive structural changes and use of the more powerful J75 were deemed significant enough to warrant redesignation. Externally evident changes from the F-102 are the square-tipped vertical stabilizer, repositioning of the air intakes farther aft, more pronounced area-ruling of the fuselage, more sweep on the delta wing, and the cockpit, which is farther forward for improved pilot visibility. Figure 25(a) is a three-view drawing of the aircraft. The

primary armament for the Delta Dart interceptor, air-to-air rockets, is carried internally in a weapons bay. Both single- and two-place versions were built. Data from reference 16 on the F-106A single-cockpit model are used in this study.

The F-106 is a tailless design, capable of speeds to Mach 2.0. The trailing-edge flaps, called elevons, are used for trim as well as pitch and roll control. Trim is accomplished by reflex, or reversed, camber of the wing. Therefore "trim drag" must be computed by different means than with conventional aircraft equipped with horizontal tails. The F-106 can shift fuel to relocate the center of gravity to reduce trim drag during supersonic flight, a complexity that is not required for conventionally configured fighters.

XB-70 Valkyrie

The XB-70 Valkyrie, a very large aircraft designed as a supersonic-cruising strategic bomber, is characterized by its delta wing and canard. Although production of the B-70 was judged infeasible, three XB-70As were built and tested as aerodynamic research aircraft. The Valkyrie was designed to cruise at Mach 3; the wing tips fold down hydraulically to improve stability and maneuverability. Twin vertical fins with large, angle-hinged rudders are mounted atop the delta wing, and rectangular cross-section intake ducts are mounted below the wing to provide air to the six YJ93 afterburning turbojet engines. The inlet system also positions the shock wave to produce a favorable interaction that remarkably increases the supersonic lift/drag ratio. The large canard foreplane is adjustable for trim purposes and is fitted with trailing-edge flaps, which make it possible to droop the elevons on the wing trailing edge to act as flaps for takeoff and landing. Figure 26(a) details the layout of the XB-70; the aerodynamic data shown in figure 26(b) are from reference 17.

COMPARISONS OF MEASURED AND PREDICTED TRIMMED LIFT-DRAG POLARS

Inputs

The aircraft geometry inputs required for the AEROX program (listed in ref. 2) include the area; sweep; thickness-to-chord ratio; aspect ratio and taper ratio of the wing and horizontal tail; tail length; lengths and diameter of the nose and fuselage; and the center-of-gravity location. Two unique inputs which relate the aircraft to the appropriate AEROX flow zones and equations are (1) the aforementioned airfoil designator J or specification of the effective leading-edge radius-to-chord ratio, ROC, and (2) the chordwise shock location XCD when zone 4 conditions exist. Available or estimated values of minimum drag coefficient C_{D_o} and of camber-offset lift coefficient C_{L_B} (fig. 5(a) and table 2) are also input. Of the camber inputs, only the value of 0.14 for the A-7 exceeded 0.1, with the others being very small or zero.

The airfoil designators of $J \leq 4$ enable the program to select the appropriate leading-edge radius, for calculating flow zones and aerodynamic equations. If the airfoil employs a leading-edge device, such as a slat or droop, the effective leading-edge radius is usually increased, and a $J = 5$ designator with the specified ROC (typically near 0.02) is used for those Mach numbers at which the device is properly deployed. The right-hand column of table 2 lists four aircraft with leading-edge devices deployed at Mach numbers of 0.4 or greater, namely, the A-4, the RA-5, the A-7, and the F-8. Improved characteristics were realized on the A-4 and F-8 and the extended compressible aerodynamic zone 2 ordered in the program by the $J = 5$ designator gave predictions in agreement with the flight data. The leading-edge devices on the RA-5 and the A-7 (fixed droop) improved cruise performance; however, the sharp ridges formed at the juncture of the device and wing upper surface resulted in degraded lift-drag ratios at higher C_L's, characteristic of sharp leading edges at the higher Mach numbers. The $J = 1$ designator was used for the A-7 at all the Mach numbers covered by the data, because the droop was permanently fixed on the wing. The $J = 1$ was used only up to Mach numbers at which the device was either deployed, or suspected of deforming to produce an abrupt discontinuity in the upper profile, the latter occurring at some Mach numbers for the A-3 and the F-100.

A leading-edge device for use at high subsonic Mach numbers should generally increase the leading-edge radius and delay the onset of local Mach-limited flow around the nose or at the juncture with the upper surface of the wing. This will extend the compressible zone 2 to higher lift coefficients and offer the advantage of reduced drag, as depicted in figure 7(b). Further extension of zone 2 will require the delay of the onset of the surface Mach-limited flow zone 4. The latter requires an aft movement of the upper surface shock, that is, an increase in XCD. This is more difficult, in that the maximum cross-sectional area must be moved aft, or an aft loading on the wing, such as characterizes the supercritical airfoil, must be incorporated. Supercritical airfoils are specified in AEROX by the suitable inputs of J, ROC, and XCD.

Summary of Accuracies

The extensive collection of flight-test data was taken from the data-substantiation reports of references 4 through 19 and from some unpublished sources. These data would be expected to display some degree of inaccuracy and scatter, because of the difficulties in measuring in-flight drag and thrust, and because of the differences in aerodynamic data reduction methods used by the many companies and agencies involved. The comparisons of AEROX estimates with the large number of aircraft cases provide a reliable assessment of the program.

Table 3 presents a summary of the average accuracies of the predictions for all of the aircraft. Most of the estimates agree with flight data within ±4%.

The measured and predicted flight polars for the aircraft listed in table 1 are shown in the "(b)" parts of figures 10 through 26; the "(a)" parts of these figures are sketches of the airplanes. The flight data are solid lines, and the AEROX predictions are the broken lines. The Mach numbers and some airfoil J designators are indicated on the figures.

T-2 Buckeye

Figure 10(b) compares flight-test data with AEROX predicted lift-drag polars. At operating speeds of the aircraft ($M < 0.75$) the estimates and the test data agree so closely that differences are barely discernible. At Mach 0.75 and 0.8 the test data show increasingly more drag than that predicted, with increasing lift coefficient until the "breaks" in the prediction curves, at which time the two begin to reconverge. The "breaks" occurring at $C_L = 0.68$ ($M = 0.75$) and 0.28 ($M = 0.8$) mark the direct transitions from flow zones 2 to 4. The relatively large (12%) thickness-to-chord ratio of the T-2 wing precludes the onset of leading-edge Mach-limited flow (zone 3). The disparity at the intermediate lift coefficients of the two highest Mach numbers suggests that limit Mach numbers are being reached locally on the inboard portions of the wing as a result of the low fineness ratio of the fuselage, which would not occur if the aircraft had been designed for transonic or supersonic flight. This additional drag exhibited by the actual aircraft can be considered a potential improvement of eliminating the mutual interference. But this is unnecessary, because these two higher Mach numbers are considerably above the operational speeds of the Buckeye.

T-37 Tweety Bird

The T-37 had the greatest wing thickness-to-chord ratio of all aircraft in the study, 18% at the root decreasing to 12% at the tip. Figure 11(b) compares the T-37 flight-test data with the AEROX predicted lift-drag curves. Just as with the T-2, there are regions in which the measured drag exceeds the predicted drag considerably, but these are limited to areas of the flight envelope beyond which the aircraft is capable of sustaining steady-state flight.

In addition to the thicker airfoil section, the T-37 also has a lower fuselage fineness ratio than the T-2 and engine nacelles built into the wing roots, which accentuate the mutual interference. Deviations are expectedly more prominent and occur at even lower Mach numbers. In the absence of body interference, the flow should shift directly from zone 2 to zone 4. At Mach 0.75, where reaching of the Laitonian limit would be predicted for the wing of its own accord, the AEROX prediction is 100% accurate.

A-3 Skywarrior

Figure 12(b) depicts the predicted and flight-test lift-drag curves for the A-3. At the two lowest Mach numbers (0.5 and 0.65) estimates using

J = 3 and J = 1 are both shown. J = 1, which normally represents a sharp-nosed airfoil, gives decidedly closer results. As explained in the aircraft description section, the A-3 is equipped with automatic leading-edge slats. Devices of this type, which work fine at cruise C_L's and at lower airspeeds when deployed, are susceptible to unporting, causing a discontinuity that spawns leading-edge Mach-limit flow prematurely. The flow effects of the under-wing-mounted engines, another detail that is not accounted for in AEROX, could also be contributing to the under-prediction of drag; however, the automatic slats are a more likely cause. This suposition is based on similar phenomena displayed by other aircraft with automatic leading-edge devices. Satisfactory agreement between test data and predicted values is shown at higher Mach numbers using J = 3, the normal designator for the NACA 6-series airfoil used on the A-3.

A-4 Skyhawk

Figure 13(b) shows the lift-drag curves for the A-4 aircraft for Mach numbers from 0.5 to 0.95. The 0005 airfoil section on the A-4 is represented by J = 2; however, the A-4 is equipped with automatic leading-edge slats, just as was the A-3. At Mach numbers $\leq$0.7 the J designator is set equal to 5, and the leading-edge radius-to-chord ratio, ROC, is specified as 0.0225. This factor, which controls the onset of zone-3 flow, is between the leading-edge radius of J = 2 and the sharp leading edges of J = 1. For the full region of the flight envelope shown in figure 13(b), the slats are supposed to be fully closed, according to reference 6; our assumption of some discontinuity causing early onset of Mach-limited flow is conjecture.

RA-5 Vigilante

The RA-5 does not have automatic leading-edge slats, but does have a variable camber feature called "cruise droops," which improves L/D subsonically. These devices displayed an effect very similar to that of the automatic slats, and J = 1 was used subsonically for the AEROX calculations. Included in figure 14(b) is the calculation using J = 3 at Mach 0.4 to contrast the difference this factor makes. It must be remembered that the leading-edge factor controls the onset of Mach-limited flow and does not affect cruise performance, which normally takes place in zone 2 flow to achieve maximum aerodynamic efficiency.

At supersonic speeds the predictions are very straightforward, using J = 3 for the 65-airfoil with the leading-edge droops retracted. The accuracy of the predictions is excellent.

A-6 Intruder

Predicted and flight-test aerodynamic performance for the A-6 is compared in figure 15(b). Three different leading-edge designators are used here, because the A-6 does not have a constant leading-edge radius along the

span. The highly swept strake (see fig. 15(a)) has a sharp leading edge, and the rest of the wing has a rounded nose, 6-series airfoil section; the latter section is normally designated by J = 3, which is used at 0.8 M (near the cruise speed) and 1.3 M (fully developed Mach-limited flow). At 0.7 Mach number the J = 3 designator overpredicted the induced drag, whereas J = 5 gave close agreement. There is apparently some mechanism acting to delay the onset of leading-edge Mach-limited flow. At the transonic Mach numbers, 0.9 and 1.1, J = 1, indicative of a sharp-nosed airfoil, gave the most reasonable estimates. Here it is easier to reason the influence of the sharp leading-edge strake disturbances spreading laterally along the wing to induce easier onset of Mach-limited flow. Test data on the wing without the strake would be useful to confirm these suppositions; this example shows the usefulness of varying J as a design parameter, because once the desired flow type has been identified, the mechanism to create it can be readily sought.

A-7 Corsair II

Figure 16(b) plots lift-drag curves for the A-7. The performance of the A-7 wing is very dependent on the permanent 7° droop of the NACA 65A007 airfoil section. First, note the camber offsets used, and how the effects decrease at higher transonic Mach numbers. The second significant point is that J is set equal to 1 rather than 3, which would normally be the designator for 6-series airfoil sections. This is because of the means with which the droop was implemented with a ridge line at 20% chord as described earlier. This causes Mach-limited flow to occur at lower lift coefficients (and lower angles of attack), in this case still above those used for normal cruise. The increased drag, as can be seen by comparing the J = 5 line at M = 0.825, will only degrade maneuver performance and not cruising flight. Within the constraints of these considerations, the AEROX demonstrates good agreement at all Mach numbers; accuracies are tabulated in table 3.

F-4 Phantom II

This aircraft and the following "clean" fighter configurations have few of the anomalies encountered with the previously discussed subsonic trainer and attack aircraft. The AEROX inputs for the F-4 were straightforward, with no camber offsets or changes in airfoil designator J required. The average differences between the estimates and the flight-test data are shown for the F-4 in figure 17(b); they are less than 5%.

F-5 Freedom Fighter

Close agreement between data and estimate is evident in the results for the F-5 shown in figure 18(b). The greatest difference occurs at Mach 1.2 and is one of the few cases where AEROX has overestimated the actual induced drag. Any number of factors could account for the irregularity at this Mach number, but no particular cause is conjectured.

F-8 Crusader

Lift-drag polars for the F-8 are shown in figure 19(b); the comparison is very favorable. At Mach numbers of 0.8 and below, the leading-edge "cruise droops" are deployed and the $J = 5$ designator is used. For the "clean" wing ($M \geq 0.8$) the normal 6-series designator, $J = 3$ is used. Agreement is within 95% at all test Mach numbers.

F-11 Tiger

Figure 20(b) shows the trimmed lift-drag polar curves for the F-11. At the three highest Mach numbers (>0.9) the variance is a satisfactory 4% or less. At lower Mach numbers (≤0.9), the transition to zone 3 Mach-limited flow is not reflected in the flight-test data. AEROX predicts the onset of zone 3, based on the leading-edge radius of the 6-series airfoil section, which is small for the relatively thin (average 5%) wing of the F-11. Increased leading-edge radius (airfoil modification) or drooped leading edge (slats) could achieve the given performance, or it is possible that the data curves are an extrapolation along an assumption of induced drag remaining proportional to C_L^2.

F-100 Super Sabre

Figure 21(b) shows the close agreement obtained between the flight data and the estimates for the F-100. At subsonic Mach numbers, the nominal $J = 3$ designator is used to represent the NACA 65A007 airfoil. However, the data source cited the possible unporting or deformation of the automatic leading-edge slats at the high dynamic pressures encountered during the supersonic flights. The change from $J = 3$ to $J = 1$ for supersonic speeds resulted in the continued agreement, as shown in figure 21(b).

F-101 Voodoo

The data and estimates shown in figure 22(b) for the F-101 differ by less than 4%. Small camber inputs, which are listed in table 2, were used to account for the offsets indicated in the data for the modification of the NACA 65A007 airfoil. The high magnitude, relative to other aircraft, of drag coefficient shown in figure 22(b) is a result of a small wing reference area, which does not include the fillets and root extensions.

F-104 Starfighter

F-104 trim lift-drag polars are shown in figure 23(b). This aircraft, with its sharp leading-edge wing, exhibited flight polars that conform very well with those estimated by the AEROX program using the $J = 1$ designator, appropriate for sharp-nosed airfoil sections; no other additional specifications, such as camber offsets or chordwise shock location, were necessary.

F-105 Thunderchief

The calculations for the F-105, plotted in figure 24(b), were straightforward, using the normal $J = 3$ for the 6-series airfoil. Estimated drags were 8% high for higher lift coefficients at Mach numbers 1.0 and 1.2. This anomaly appears to be akin to that of the F-5 at Mach 1.2. At supersonic Mach numbers the drag coefficients estimated by AEROX were within 4% of the flight-derived values.

F-106 Delta Dart

The estimated drag coefficients shown in figure 25(b) for the F-106 were closest to the flight data at supersonic speeds, but were as much as 10% high at the higher lifts for the subsonic speeds, using the $J = 2$ designator for the NACA 0004 airfoil and neglecting the conical camber on the wing leading edge. Improved agreement at these high lift conditions would have resulted if the $J = 5$ designator and a larger leading-edge radius were used. Camber offsets could also be used to better the agreement. These extra estimates were not employed and no estimate is included for Mach 2.0, because the center-of-gravity location and the amount of elevon deflection required for trim were not specified. Trim drags, especially on a tailless configuration, are more significant than flow effects.

XB-70 Valkyrie

The XB-70 canard was sufficiently remote from the wing to be categorized as an uncoupled canard. The upwash and downwash field interactions between the wing and canard were considered small enough to ignore. The estimated drag coefficients used the $J = 1$ sharp-airfoil designator and no camber offsets, which produced results about 6% higher than the derived flight data shown in figure 26(b).

CONCLUSIONS

These comparisons of the aerodynamic predictions of additive (induced drag plus trim drag) drag made by the AEROX computer program with the flight-test data of 17 different aircraft have shown the following:

1. The predictions made by the AEROX programmed method generally varied less than ±4% from the flight-test data, a very acceptable value for all except the most detailed analysis.

2. The differences between the predictions and test data were more commonly due to specializations unique to the configuration than to errors in the method.

3. The effects of configuration variables like leading-edge devices, flaps, canards, camber, etc., can be accounted for within AEROX by appropriate use of the available input parameters and program options.

4. Results from this study provide useful guides for the selection of AEROX indicators of local Mach-limited flow onset and chordwise shock location for future studies.

5. Onset of Mach-limited flow also correlated very well with the buffet onset for those aircraft for which buffet onset data were available.

REFERENCES

1. Axelson, John A.: Estimation of Transonic Aircraft Aerodynamics to High Angles of Attack. AIAA Journal of Aircraft, vol. 14, June 1977.

2. Axelson, John A.: AEROX – Computer Program for Transonic Aircraft Aerodynamics to High Angles of Attack. NASA TM X-73,208, 1977.

3. Feagin, R. C.: Transonic Aircraft Drag Technique Applied to Military Aircraft. Contract NAS2-8612 for NASA Ames Research Center by Lockheed-California Company, Mar. 1977.

4. Elliott, D. W.: Substantiating Data Report Based on Flight Test Data for the T-2B Trainer Powered with Two T60-P-6 Engines. Report NA64H-536, North American Aviation, Inc., 7 June 1964.

5. Performance Data for the Model A3D-2, 2P and 2Q Airplanes Based on Flight Test Data. Douglas Aircraft Company, Inc., 29 Apr. 1960.

6. Performance Data for the Model A-4F Aircraft. Report MDC J 1087, McDonnell-Douglas Aircraft Company, 23 Feb. 1971.

7. Performance Substantiating Data Report for the RA-5C Aircraft with J79-GE-10 Engines. North American Rockwell Corp., 27 Feb. 1969.

8. Ohler, J. C.: A2F-1 (A-6A) Basic Data Report for the Standard Aircraft Characteristics Chart of August 1959. Report XA128-105-3, Grumman Aircraft Engineering Corporation, Aug. 1959.

9. Miles, R. B.: Model F-4E Performance Data and Substantiation. Report MDC A1158, McDonnell Aircraft Company, 20 July 1971.

10. Ackerman, N. G.; and Warren, B. L.: F-5 Basic Aerodynamic Drag Data. Report NOR-64-2, Northrop Corporation, Jan. 1964.

11. Artificavitch, W. P.: F8U-2 (F-8C) Performance Data. Report E8R-11402, Chance Vought Aircraft, 19 May 1958.

12. Nugent, J.: Lift and Drag of a Swept-Wing Fighter Airplane at Transonic and Supersonic Speeds. NASA Memo 10-1-58 H, Jan. 1959.

13. Chewning, N. C.; Vondrasek, D.; and Beeler, N.: Model F-101B Flight Manual and Standard Aircraft Characteristics. Report 6907, vol. I, McDonnell Aircraft Corporation, 30 Dec. 1960.

14. Avant, N. T.: Map F-104G Performance Characteristics. Report LR 16097, Lockheed Aircraft Corporation, 16 July 1962.

15. Smith, L.; and Margolin, M.: Substantiation Report for the F-105D Aircraft. Report 1171, Republic Aviation, Mar. 1963.

16. Flight Performance Manual – Performance Data for the F-106A and F-106B. Report T.O. 1F-106A-1, General Dynamics Convair Aerospace Division, 1 Dec. 1972.

17. Estimated Performance and Drag Substantiation Report for the B-70 Primary Air Vehicle. Report NA-59-268-1, North American Aviation, 1959.

18. Wong, F. T.: Model T-37B Substantiating Data for Standard Aircraft Characteristics Charts, Based on Category II Flight Test Data. Report 31813-7003-120, Cessna Aircraft Company, 21 Dec. 1970.

19. Styne, H. E.: A-7B Aircraft, Basic Data for Performance Calculation. Report 2-53330/8R-5345, LTV Aerospace Corporation, 10 Jan. 1968.

TABLE 1.- SPECIFIED CAMBERS AND CHORDWISE SHOCK LOCATIONS

Airplane	Shock locations	Camber offsets
T-2	XCD = 0.2 at M = 0.8	0
T-37	XCD = 0.6 at M = 0.7, = 0.2 at M = 0.725, 0.75	-0.10 at M = 0.75
A-3	(a)	0.03 at M = 0.50; 0.02 at M = 0.65; -0.03 at M = 0.85; -0.06 at M = 0.90
A-4	(a)	-0.04 at M = 0.90; -0.06 at M = 0.95
A-5	(a)	0.1; 0.08 at M = 0.40, 0.80; 0.90; (J = 1) -0.03 at M = 1.3 (J = 3)
A-6	(a)	0.05 at M = 0.80
A-7	(a)	0.14 at M = 0.825, 0.90; 0.10 at M = 0.925; 0.08 at M = 0.95
F-4	(a)	0
F-5	(a)	-0.03 at M = 0.60
F-8	(a)	0
F-11	(a)	0
F-100	(a)	0.04 at M = 0.63, 0.85; -0.02 at M = 1.03; -0.03 at M = 1.15; -0.04 at M = 1.3; -0.05 at M = 1.44
F-101	(a)	0.08 at M = 0.75; 0.05 at M = 0.9, 1.0, 1.2; 0.09 at M = 1.6
F-104	(a)	0
F-105	(a)	0
F-106	XCD = 0.4 at M = 1.2, 1.6	0
B-70	(a)	0

[a]No XCD shock location required within the available data. All camber offsets zero unless listed otherwise.

TABLE 2.- AIRCRAFT DIMENSIONAL DATA

Airplane (data figure)	Aspect ratio	Sweep c/4, deg	Taper ratio	Thickness/ chord C_L tip	c.g. location .xx $\bar{c}$	Airfoil	Designator J	Wing modification
T-2 (10)	5.07	2.2	0.50	0.120 .120	0.25	64A212	3	
T-37 (11)	6.20	0.1	.68	.180 .120	.28	24xx	2	
A-3 (12)	6.75	35.9	.34	.097 .076	.30	63-	3	Slats M ≤ 0.65
A-4 (13)	2.91	33.2	.20	.050 .050	.27	0005	5 2	Slats M ≤ 0.7
RA-5 (14)	3.73	37.5	.19	.050 .042	.30	65-	1 3	L.E. droop and ridge, M ≤ 0.8
A-6 (15)	5.31	25.0	.31	.090 .060	.25	64A2xx	5,3,1	Snarp L.E. fillet
A-7 (16)	4.00	35.0	.25	.070 .070	.28	65A007	5,1	7° L.E.; droop, ridge
F-4 (17)	2.82	45.0	.17	.064 .030	.30	000x	2	
F-5 (18)	3.75	24.0	.20	.048 .045	.12 .30	65A005	3	
F-8 (19)	3.39	42.0	.25	.060 .050	.30	65A006	5,3	7° L.E., M = 0.8
F-11 (20)	4.00	35.0	.50	.060 .040	.25	65A00x	3	
F-100 (21)	3.86	45.0	.26	.070 .070	.30	65A007	3,1	M > 1 slat; deform ridge
F-101 (22)	4.28	36.0	.29	.070 .060	.25	65A007 mod.	3	
F-104 (23)	2.46	18.1	.38	.034 .034	.30 .35	Sharp	1	
F-105 (24)	3.18	45.0	.47	.060 .040	.30	64A00x	3	
F-106 (25)	2.20	51.9	.03	.040 .040	.25	0004	2	
XB-70 (26)	1.75 1.12	58.8 58.8	.02 .24	.020 .025 .020 .025	.22 .22 ref	Sharp Sharp	1 1	Planar wing Tips 65° down

TABLE 3.- ACCURACIES OF ESTIMATED DRAG COEFFICIENTS

Airplane (figure)	Mach No.	C_L range	Average accuracy	Airplane (figure)	Mach No.	C_L range	Average accuracy
T-2B (10)	0.60	0.0-0.8	(a)	F-5A (18)	0.60	0.0-0.5	(a)
	0.70	0.0-0.8	(a)			0.5-0.7	8% low
	0.80	0.0-0.4	10% low		0.80	0.0-0.6	(a)
		0.4-0.8	(a)		1.00	0.0-0.7	(a)
					1.20	0.0-0.7	8% high
T-37B (11)	0.50	0.0-1.2	(a)		1.60	0.0-0.7	(a)
	0.70	0.0-1.2	13% low		2.00	0.0-0.6	(a)
	0.75	0.0-0.8	(a)				
A-3B (12)	0.50	0.0-0.8	12% low	F-8C (19)	0.60	0.0-0.5	(a)
	0.80	0.0-0.8	(a)		0.90	↓	(a)
	0.90	0.0-0.5	(a)		1.00		(a)
		0.5-0.7	8% low		1.40		5% low
					1.80		(a)
A-4F (13)	0.50	0.0-0.5	(a)	F-11 (20)	0.86	0.0-0.3	(a)
	0.80	0.0-0.5	(a)			0.3-0.6	20% high
	0.95	0.0-0.3	(a)		0.90	0.0-0.6	16% high
					1.00	0.0-0.6	(a)
A-5C (14)	0.40	0.0-0.4	12% low	F-100 (21)	0.63	0.0-0.7	(a)
		0.4-0.6	7% high		0.85	0.0-0.6	(a)
	0.90	0.0-0.6	(a)		1.03	0.0-0.4	(a)
	1.00	0.0-0.5	(a)		1.30	0.0-0.4	(a)
	1.30	0.0-0.4	(a)		1.44	0.0-0.3	(a)
	1.60	0.0-0.3	(a)				
	2.00	0.0-0.2	(a)				
A-6A (15)	0.70	0.0-0.8	(a)	F-101 (22)	0.75	0.0-0.8	(a)
	0.90	0.0-0.6	(a)		0.90	0.0-0.8	(a)
	1.10	0.0-0.4	(a)		1.00	0.0-0.7	(a)
	1.30	0.0-0.3	(a)		1.20	0.0-0.3	(a)
					1.60	0.0-0.3	(a)
A-7A (16)	0.825	0.0-0.7	(a)	F-104G (23)	0.80	0.0-0.6	(a)
	0.90	0.0-0.6	(a)		1.00	↓	(a)
		0.6-0.8	4% high		1.20		(a)
	0.95	0.0-0.7	(a)		1.40		(a)
					1.80		(a)
F-4E (17)	0.60	0.0-0.8	(a)	F-105 (24)	0.60	0.0-0.6	6% high
	0.80	0.0-0.8	(a)		1.00	↓	8% high
	1.00	0.0-0.7	5% low		1.60		(a)
	1.20	0.0-0.7	5% low		2.00		(a)
	1.60	0.0-0.6	(a)				
	2.00	0.0-0.5	(a)				

Note: Approximately 75% of all comparisons agreed within ±4% of the flight-test or wind-tunnel data. When no camber offset was used, 60% of comparisons were within ±4%.

[a]Within ±4%.

TABLE 3.- Concluded.

Airplane (figure)	Mach No.	C_L range	Average accuracy
F-106 (25)	0.60	0.0-0.7	(a)
		0.7-0.9	10% high
	0.80	0.0-0.7	(a)
		0.7-0.9	10% high
	1.00	0.0-0.9	(a)
	1.20	0.0-0.6	8% low
		0.6-0.7	(a)
	1.60	0.0-0.4	(a)
B-70 (26)	0.80	0.0-0.8	8% high
	1.00	0.0-0.8	10% high
	1.60	0.0-0.8	(a)
	2.40	0.0-0.7	6% high
	3.00	0.0-0.7	(a)

Note: Approximately 75% of all comparisons agreed within ±4% of the flight or wind-tunnel data. When no camber offset was used, 60% of comparisons were within ±4%.

[a]Within ±4%.

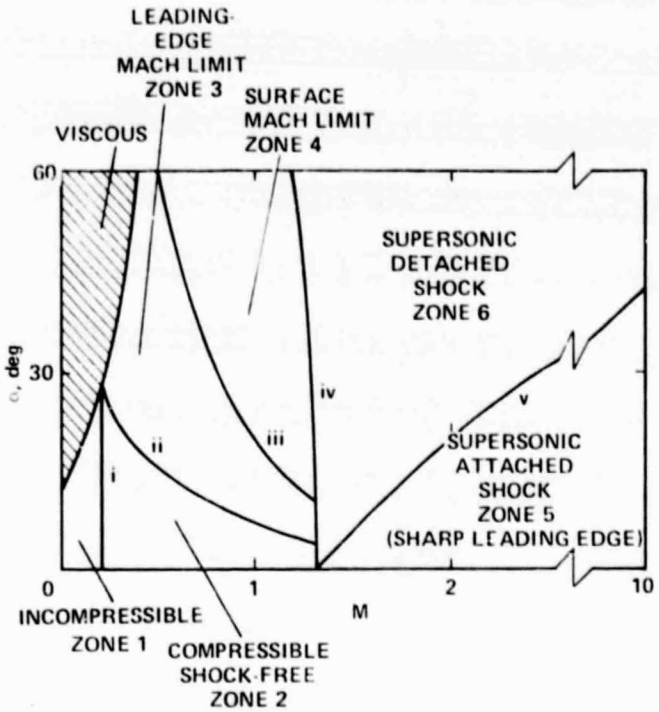

BOUNDARY	PRIMARY INFLUENCES
i	MACH NUMBER
ii	LEADING-EDGE RADIUS
iii	ANGLE-OF-ATTACK OR LIFT COEFFICIENT
iv	LEADING-EDGE SWEEP
v	ANGLE OF ATTACK (SHARP LEADING EDGE)

(a) Angle of attack vs Mach number.

Figure 1.- AEROX flow zones.

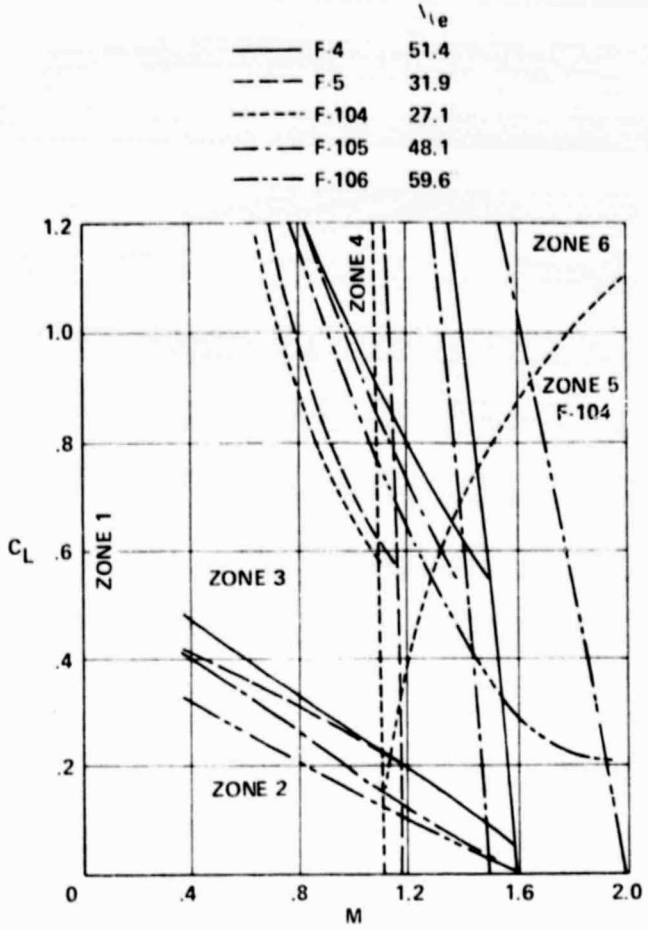

(b) C_L vs Mach number.

Figure 1.- Concluded.

(a) Zone 2: compressible potential flow, conventional airfoil.

(b) Zone 2: Compressible potential flow, extended to higher α with slat.

(c) Zone 3: Mach limit reached on leading edge.

(d) Zone 3: Mach limit reached on ridge line on airfoil with leading-edge droop.

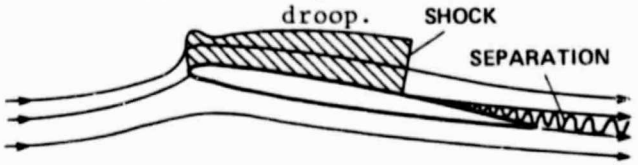

(e) Zone 4: Mach limit on airfoil upper surface.

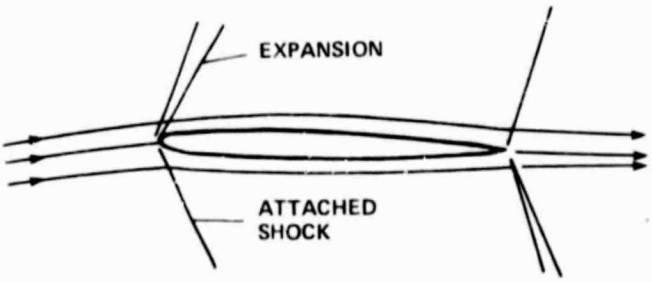

(f) Zone 5: attached shock wave.

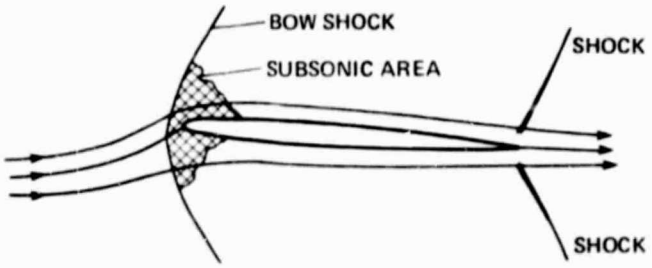

(g) Zone 6: detached bow shock.

Figure 2.- Visualizations of flow zones.

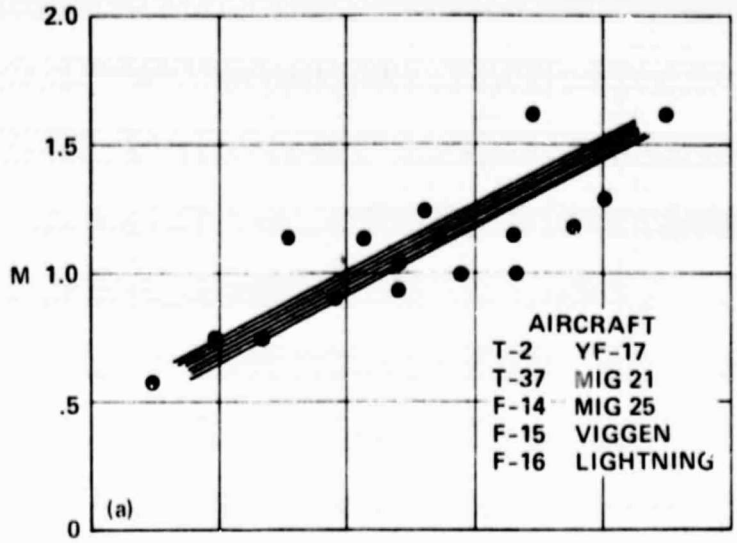

(a) Correlation of XCD with Mach number.

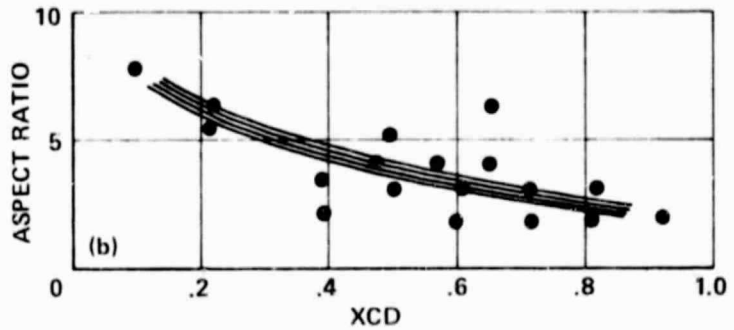

(b) Correlation of XCD with aspect ratio.

Figure 3.- Correlations of chordwise shock location XCD.

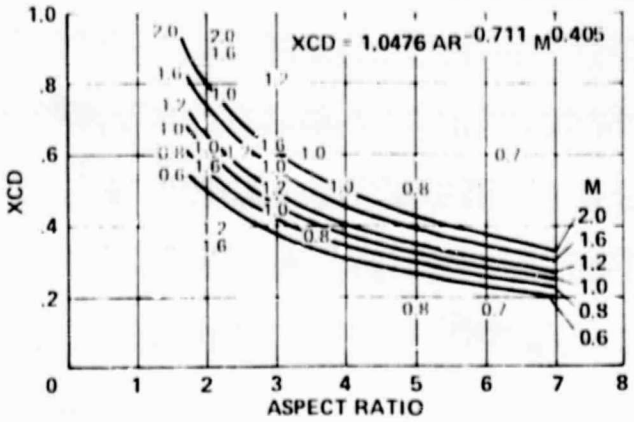

Figure 4.- Chordwise shock locations, XCD.

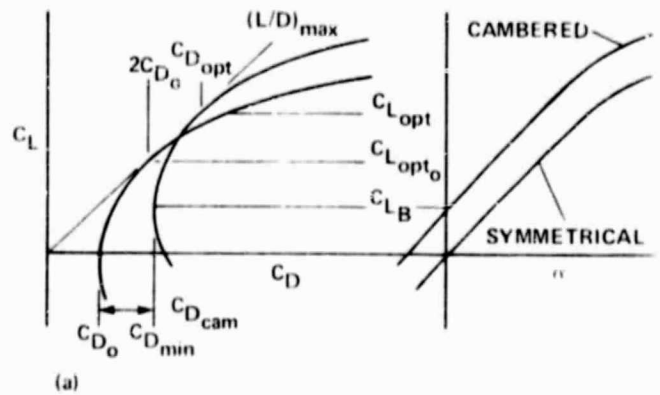

Figure 5.- Effects of camber on lift-drag polar and lift curve in subsonic compressible flow (z = 2).

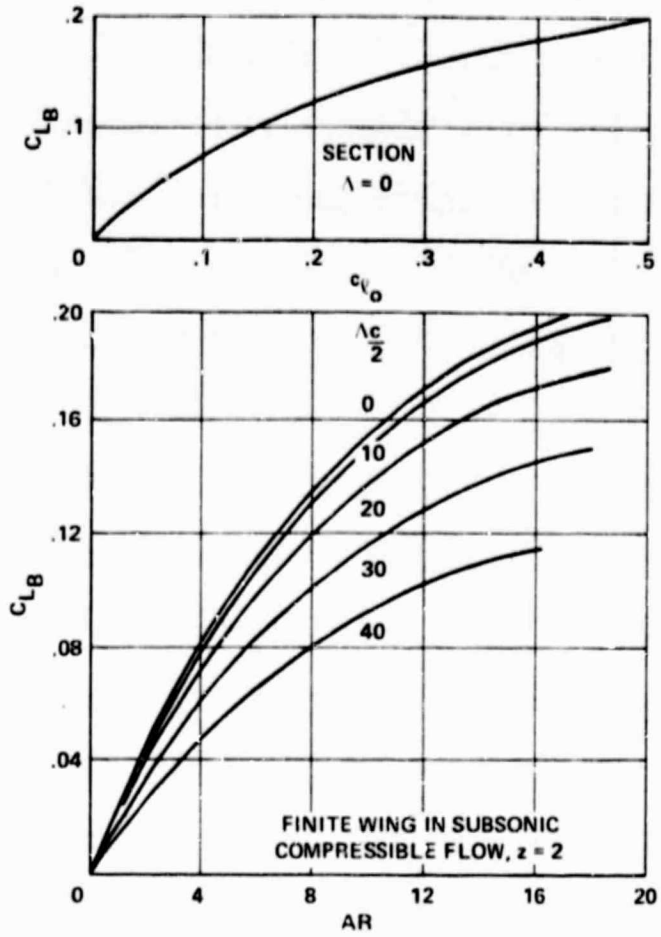

Figure 6.- Three-dimensional camber effects.

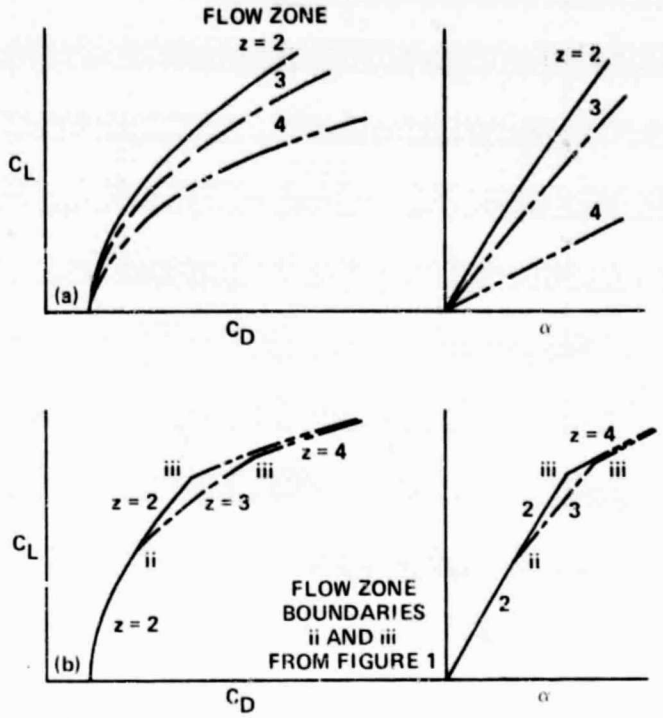

Figure 7.- Components and composite of transonic lift and drag.

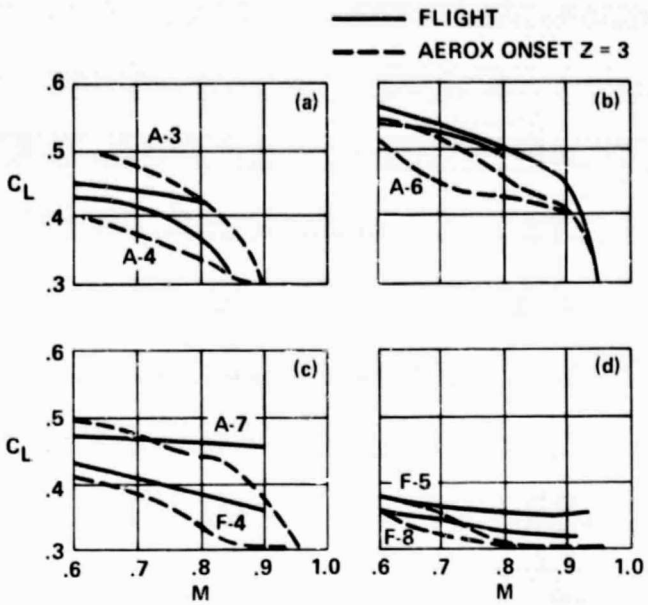

Figure 8.- Buffet onset, lift coefficient vs Mach number.

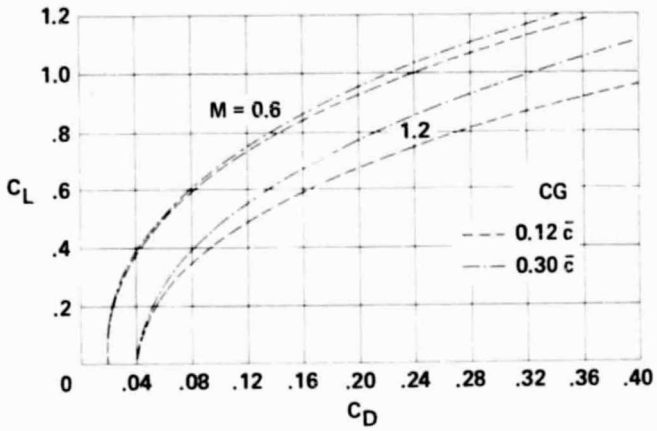

Figure 9.- Effect of center-of-gravity location on the estimated trimmed lift-drag polars.

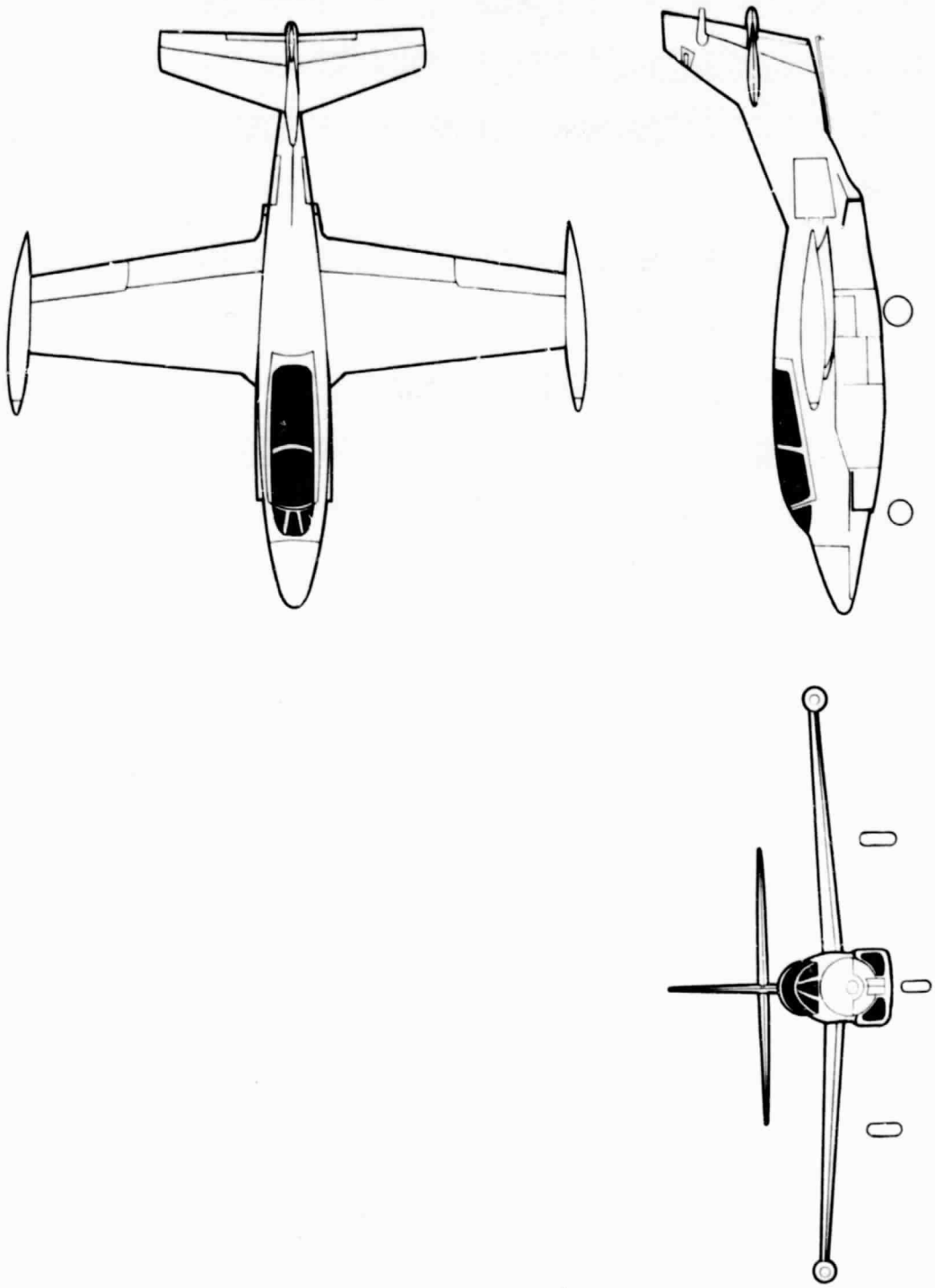

(a) Three-view.

Figure 10.- T-2.

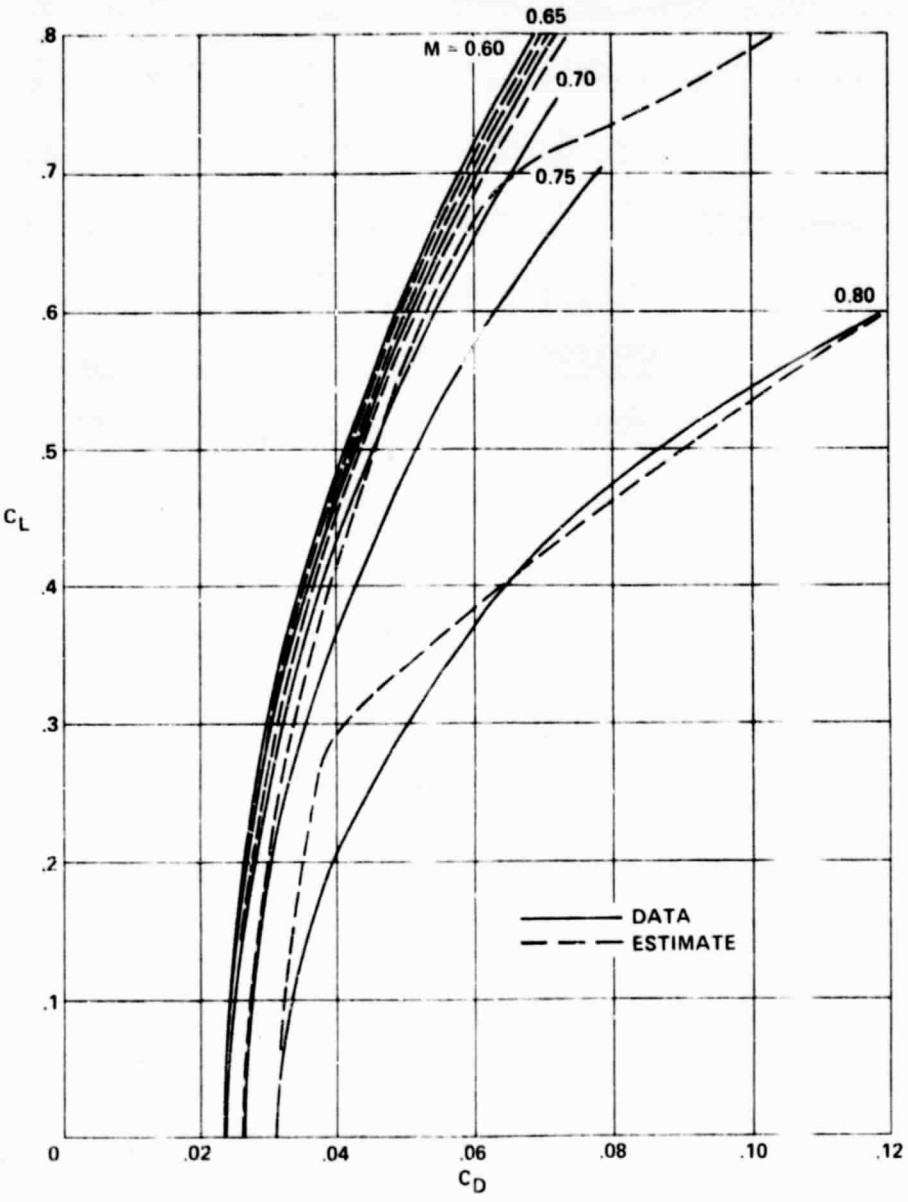

(b) Trimmed lift-drag polar.

Figure 10.- Concluded.

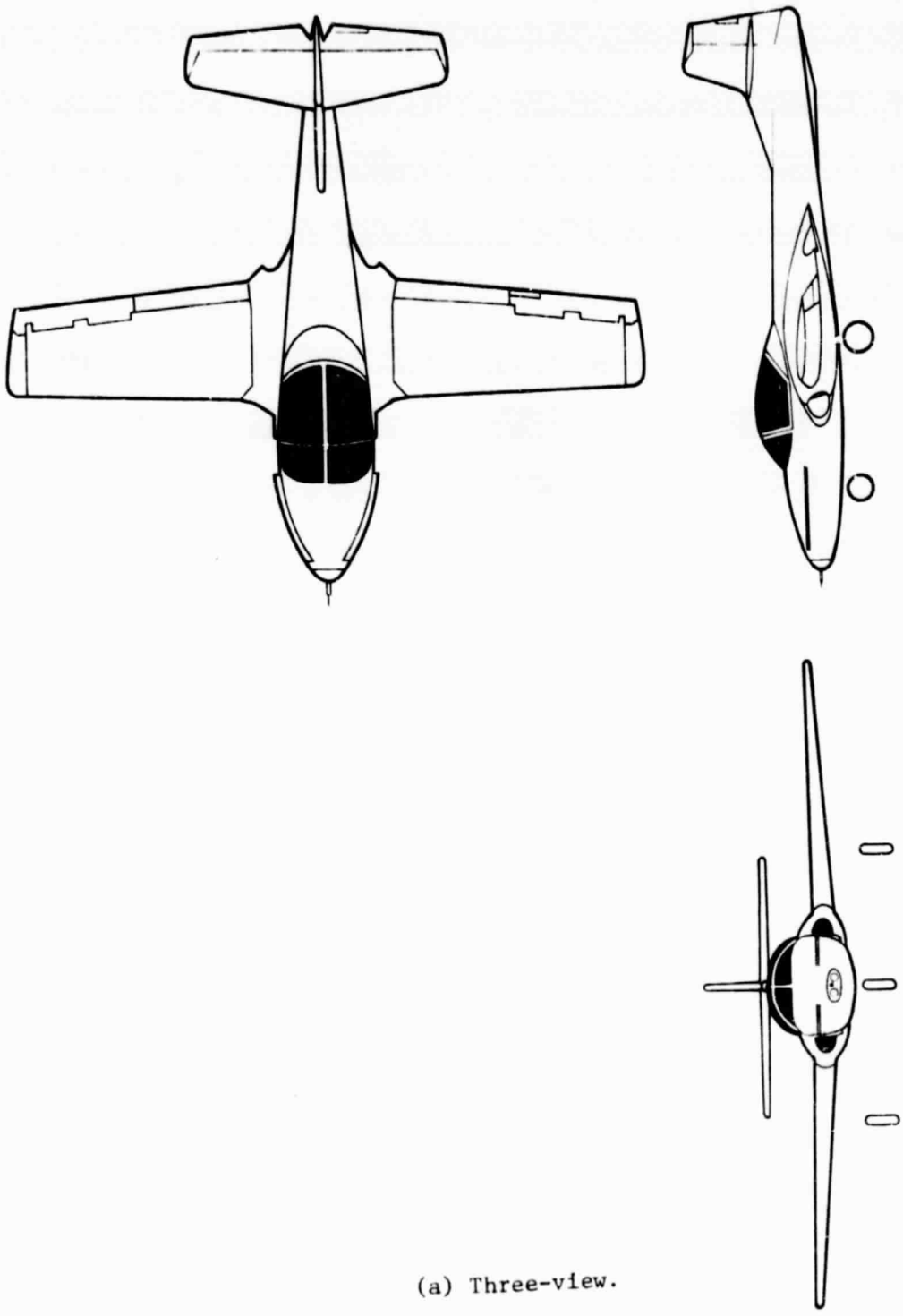

(a) Three-view.

Figure 11.- T-37.

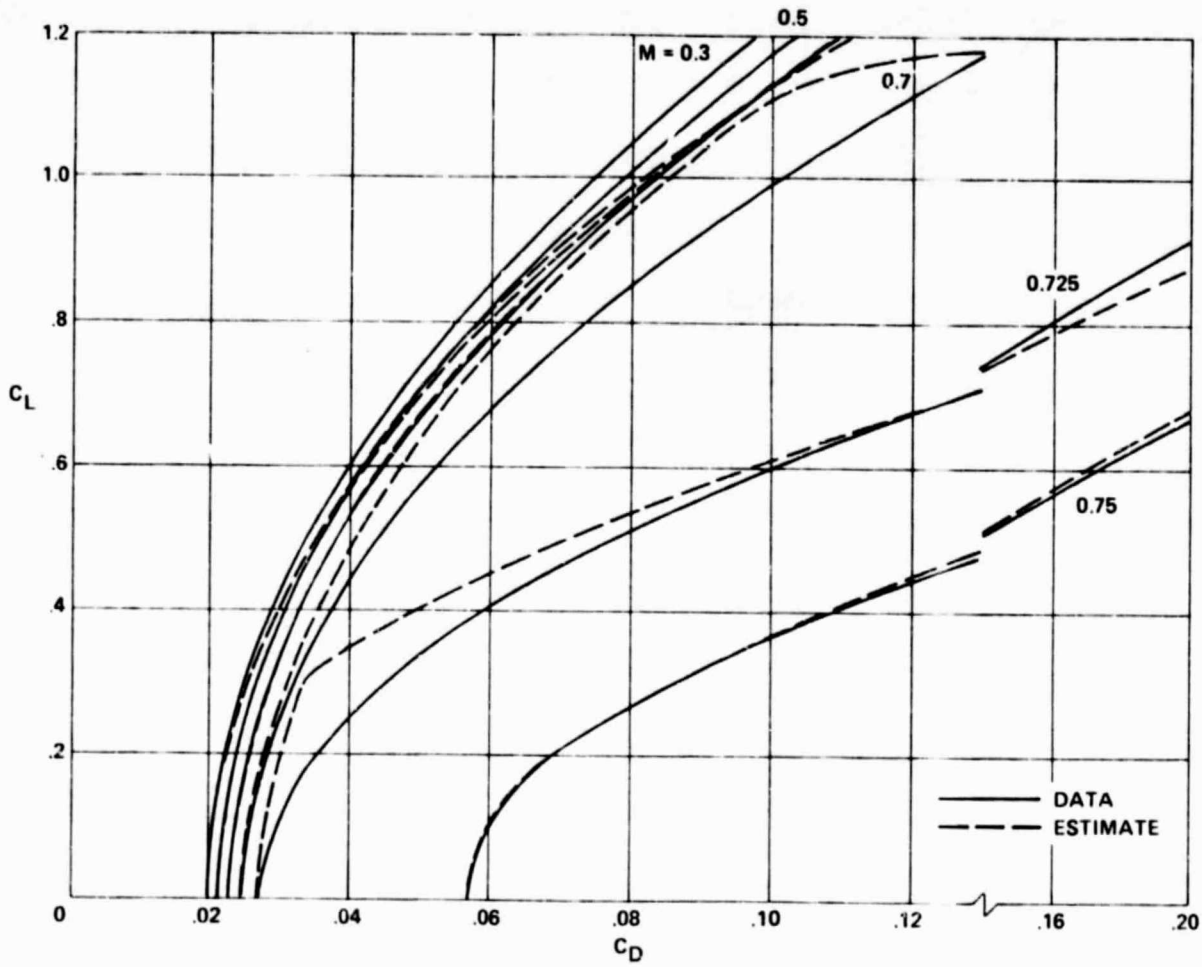

(b) Trimmed lift-drag polar.

Figure 11.- Concluded.

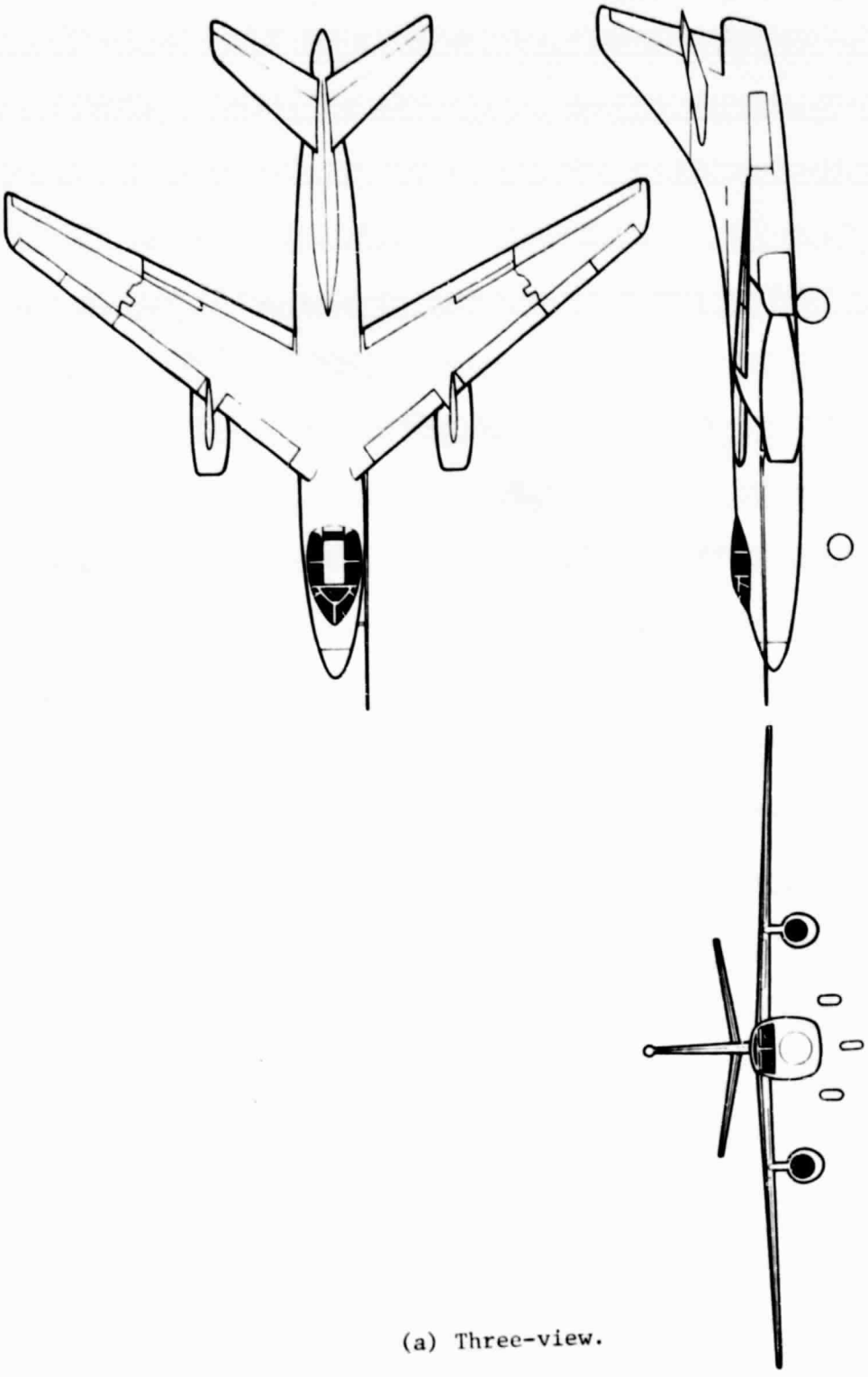

(a) Three-view.

Figure 12.- A-3.

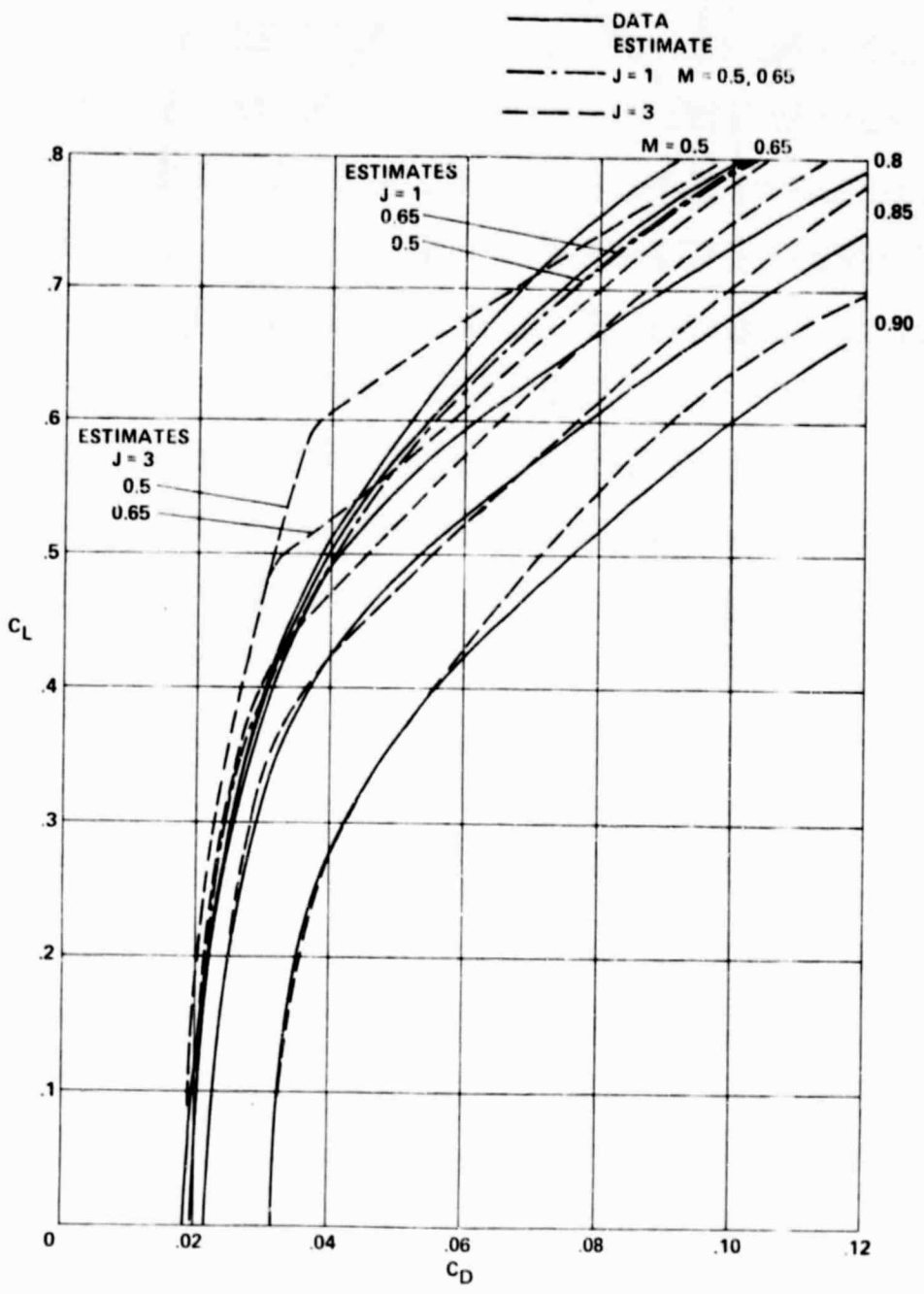

(b) Trimmed lift-drag polar.

Figure 12.- Concluded.

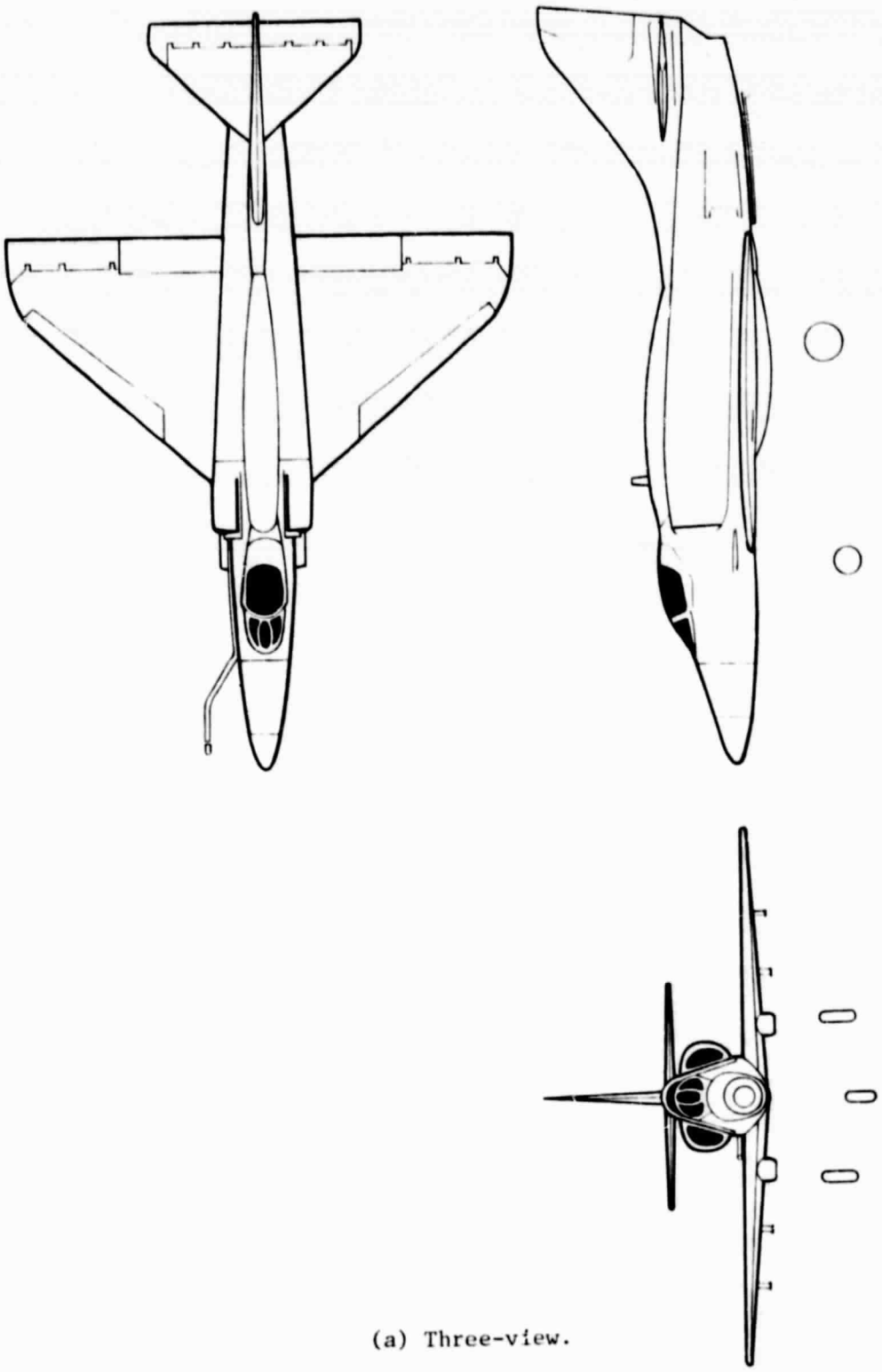

(a) Three-view.

Figure 13.- A-4.

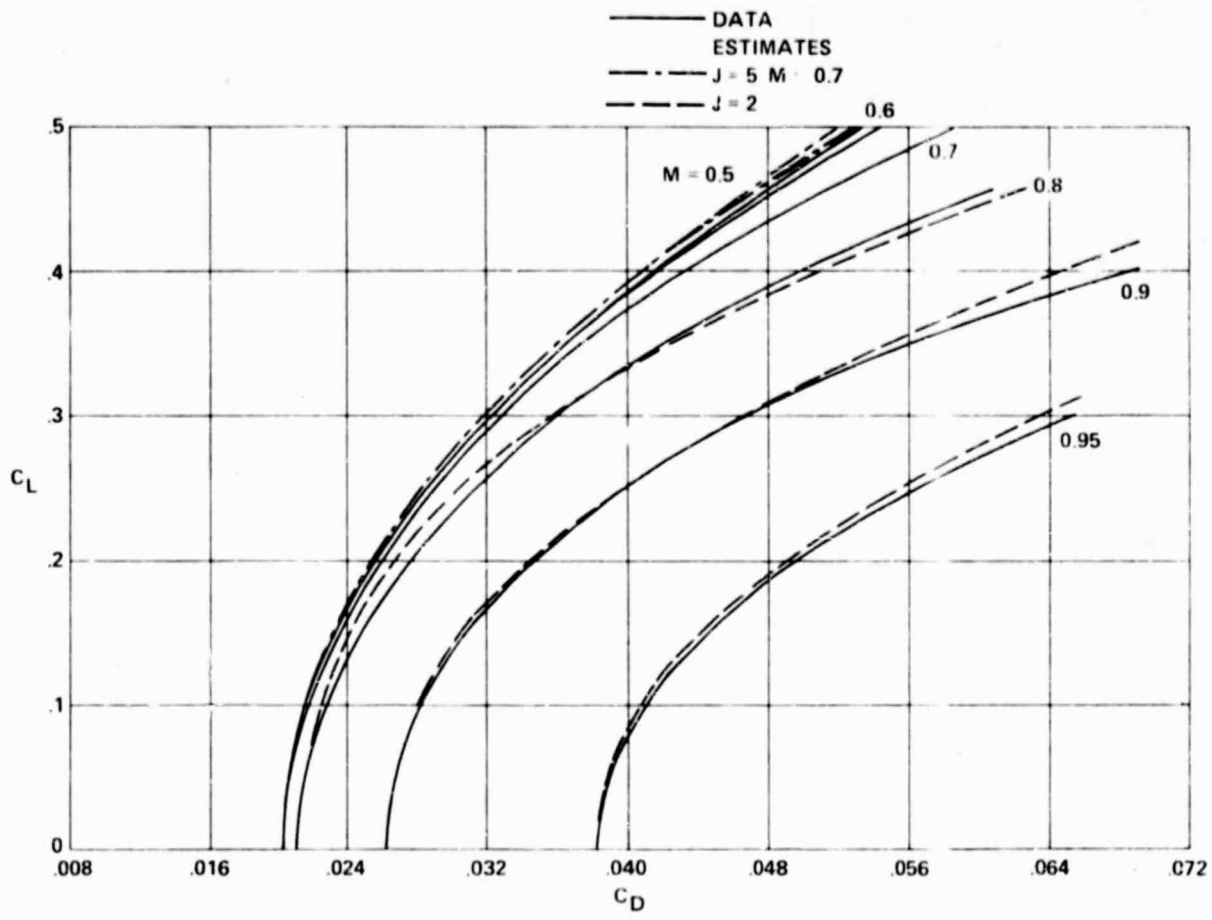

(b) Trimmed lift-drag polar.

Figure 13.- Concluded.

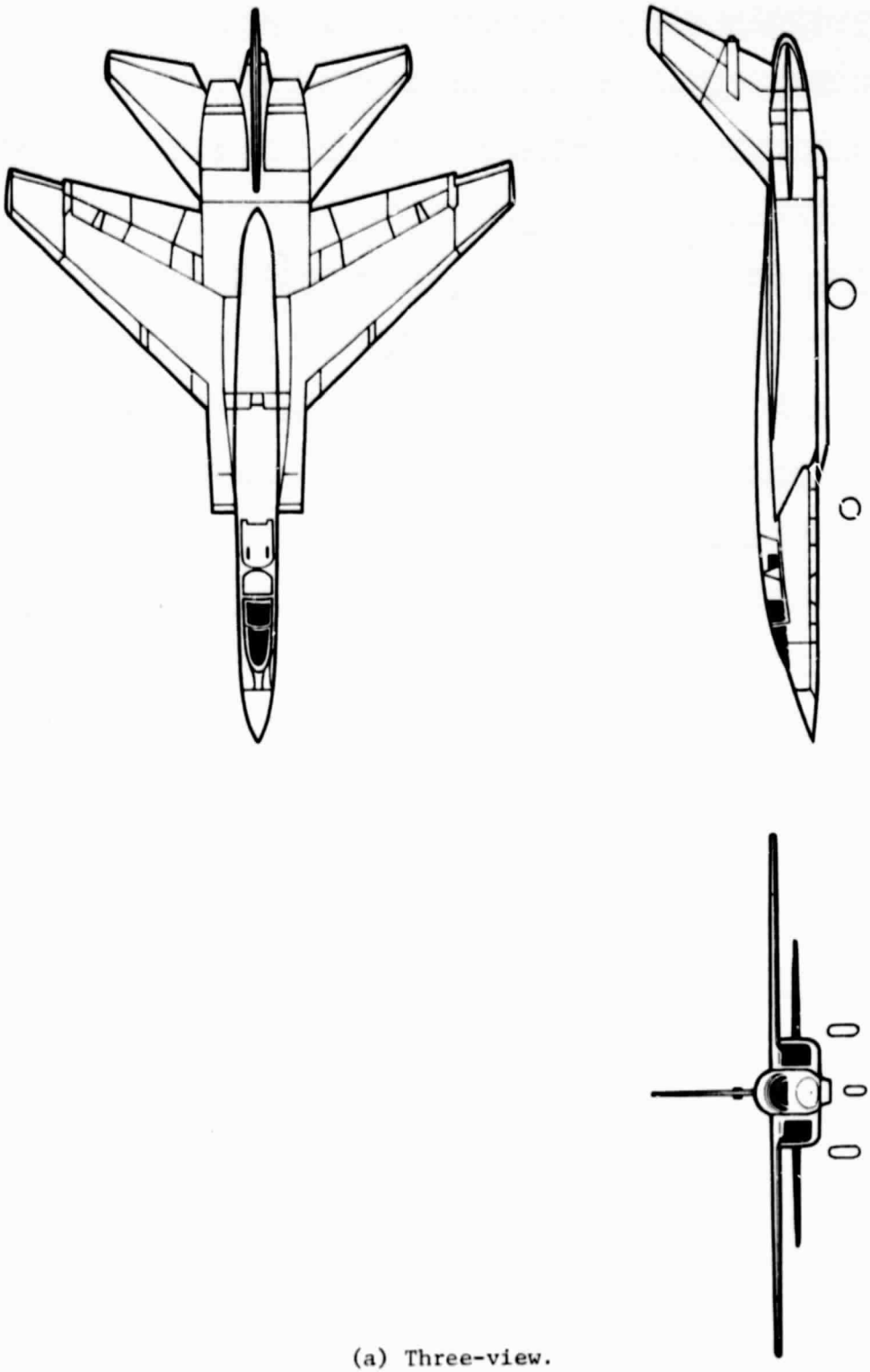

(a) Three-view.

Figure 14.- RA-5.

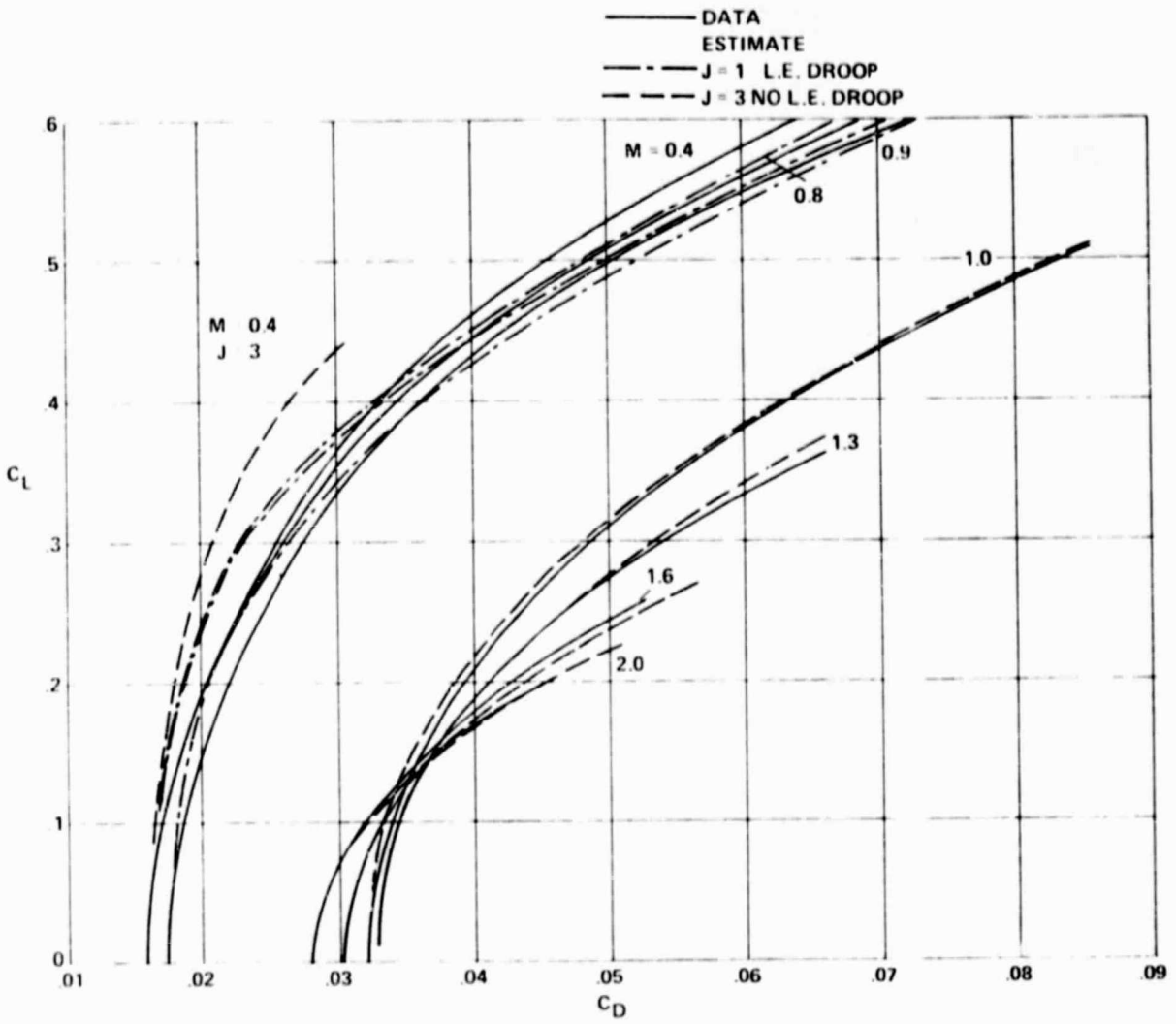

(b) Trimmed lift-drag polar.

Figure 14.- Concluded.

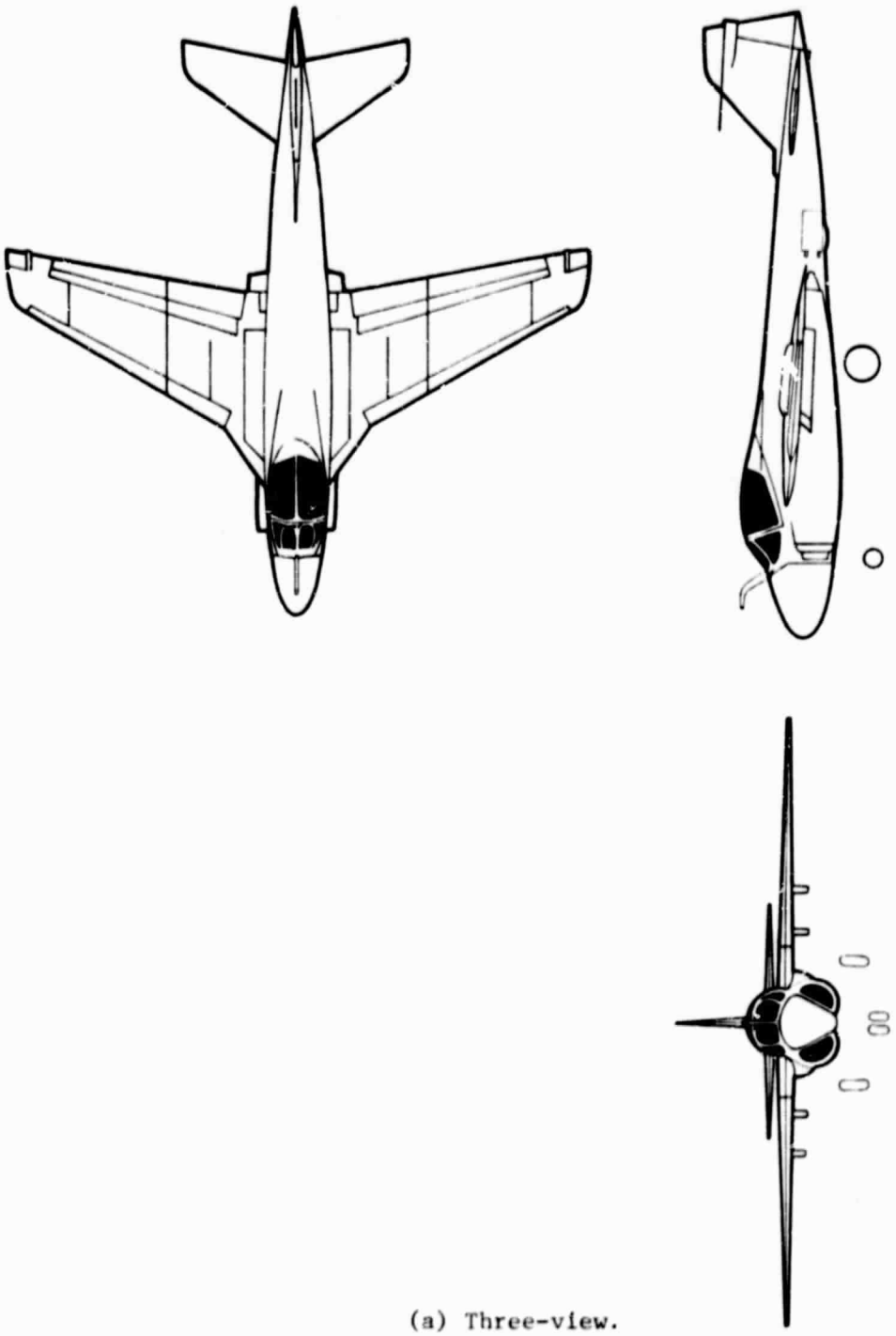

(a) Three-view.

Figure 15.- A-6.

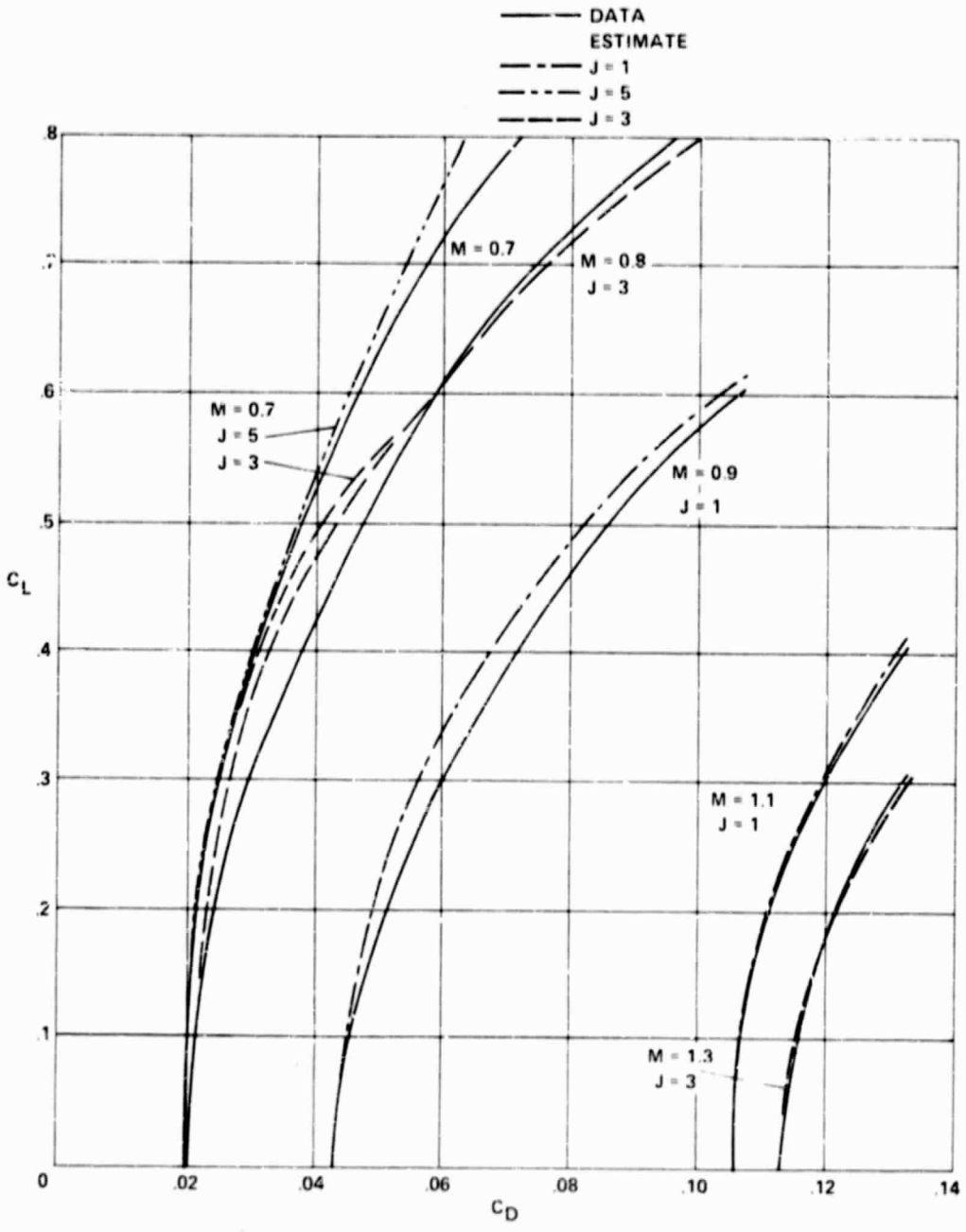

(b) Trimmed lift-drag polars.

Figure 15.- Concluded.

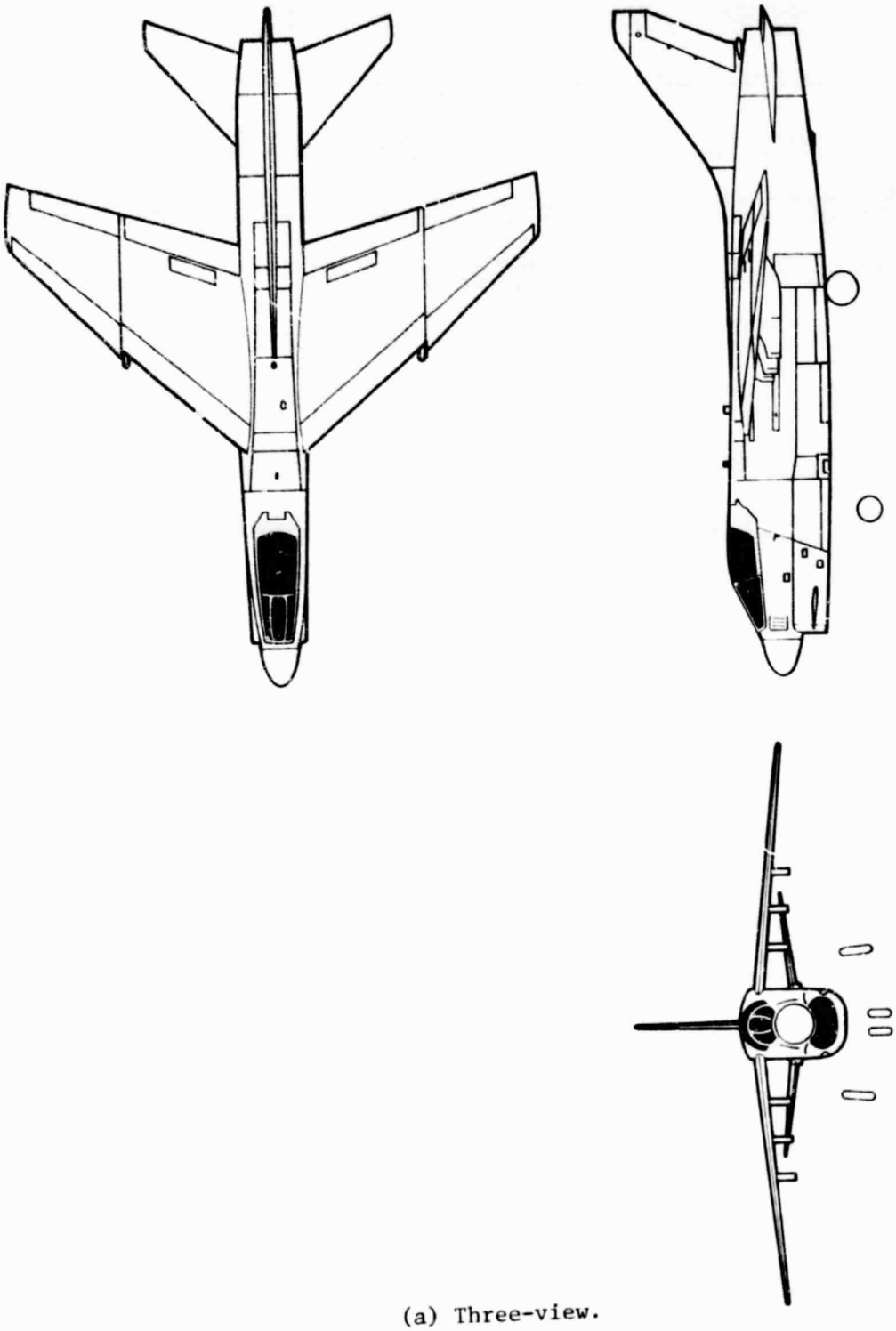

(a) Three-view.

Figure 16.- A-7.

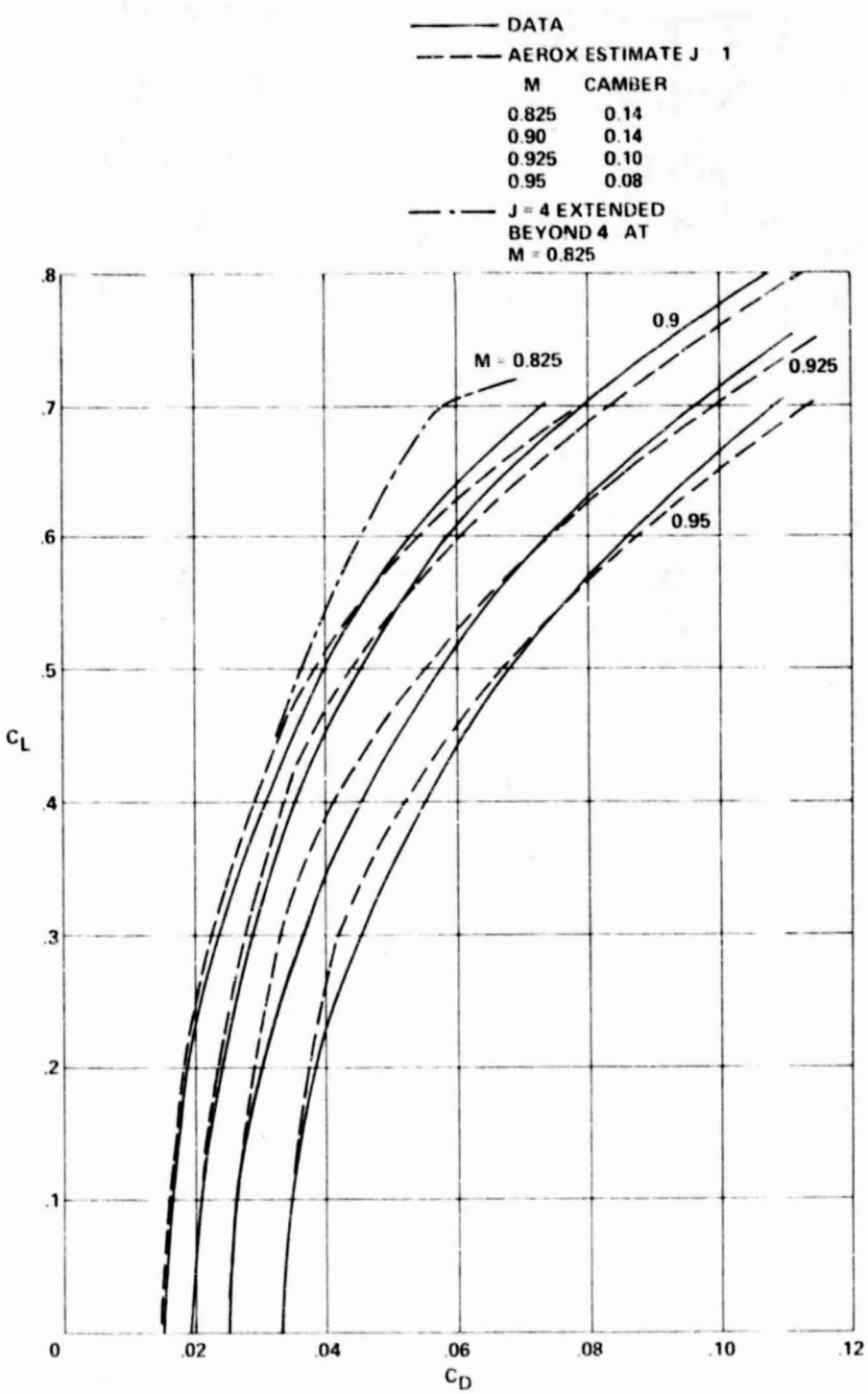

(b) Trimmed lift-drag polars.

Figure 16.- Concluded.

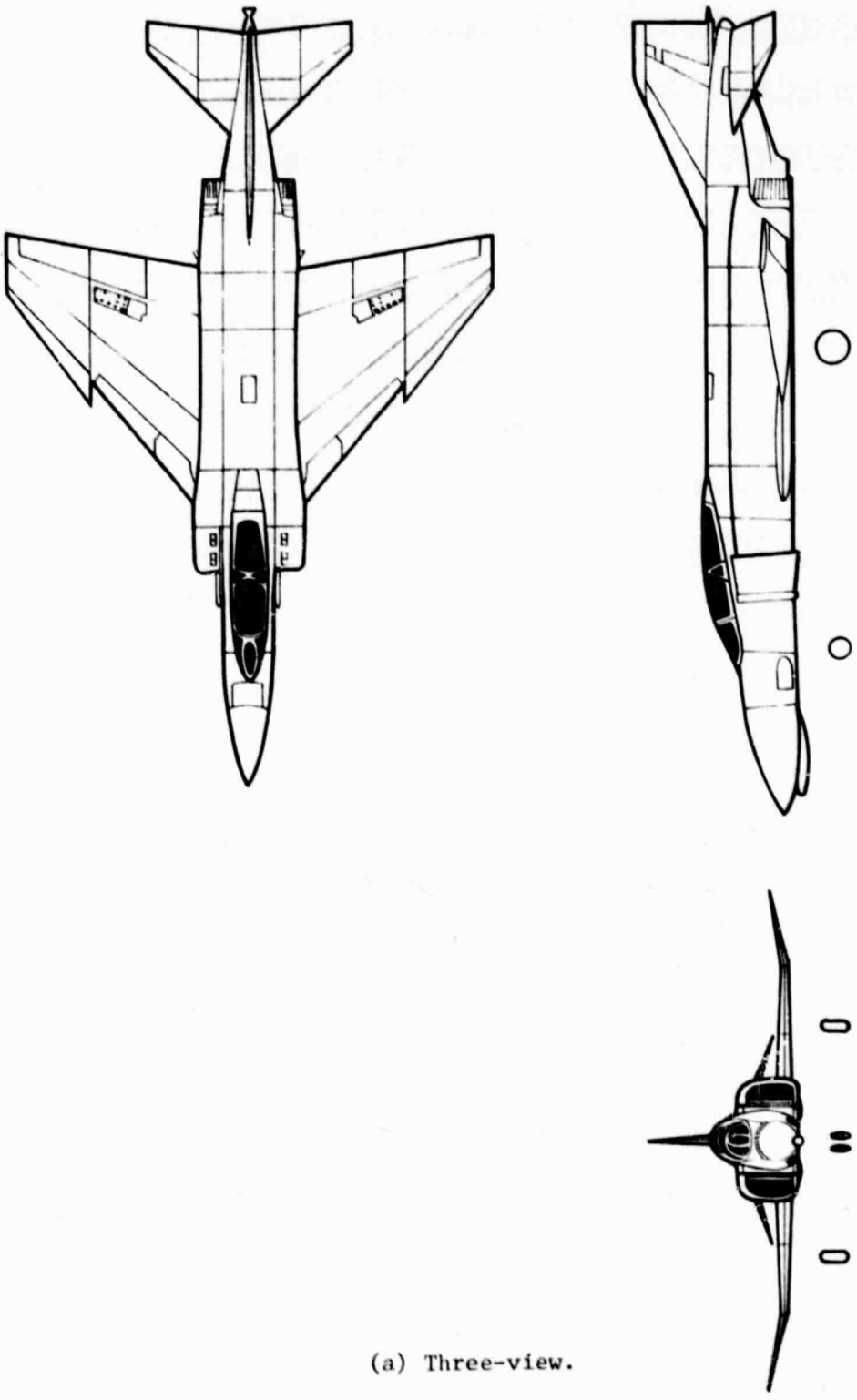

(a) Three-view.

Figure 17.- F-4.

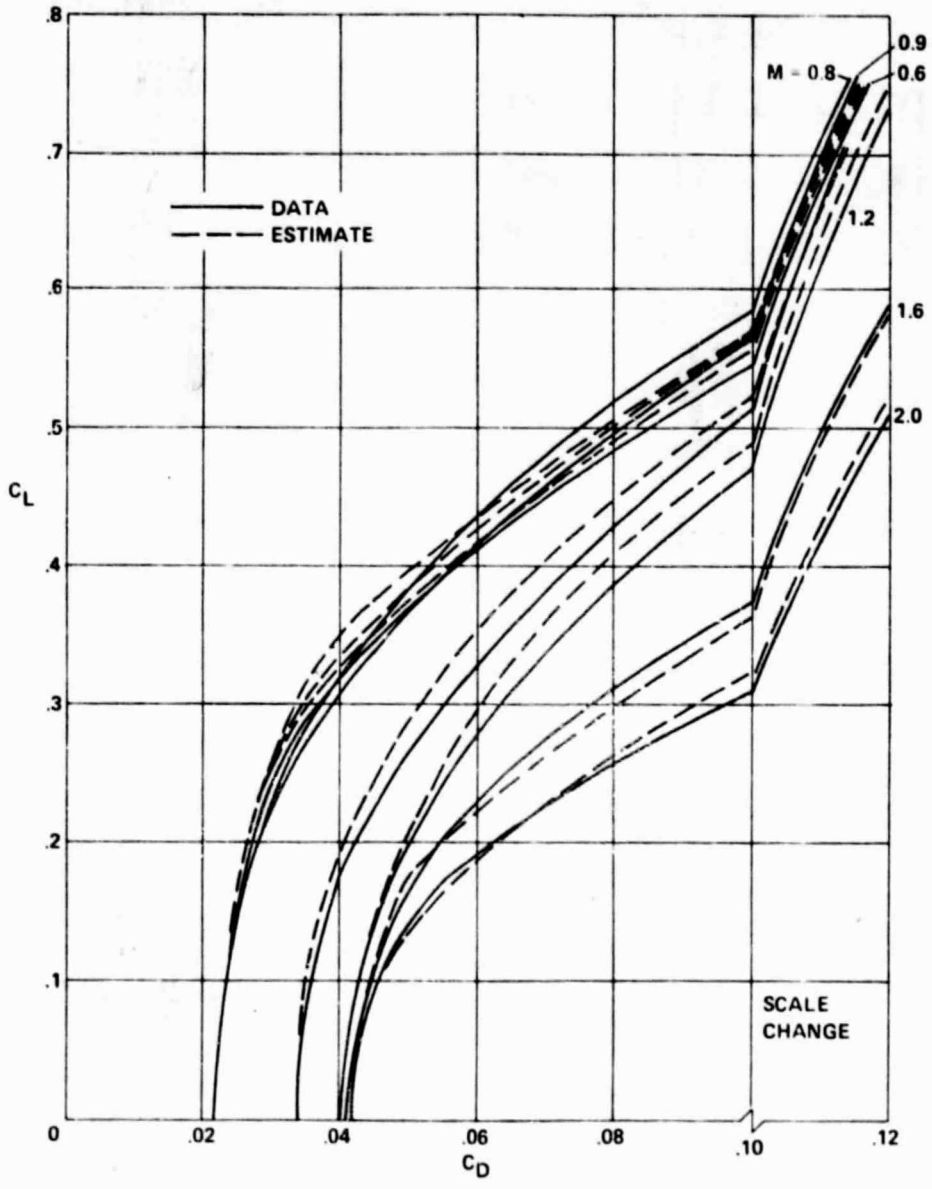

(b) Trimmed lift-drag polars.

Figure 17.- Concluded.

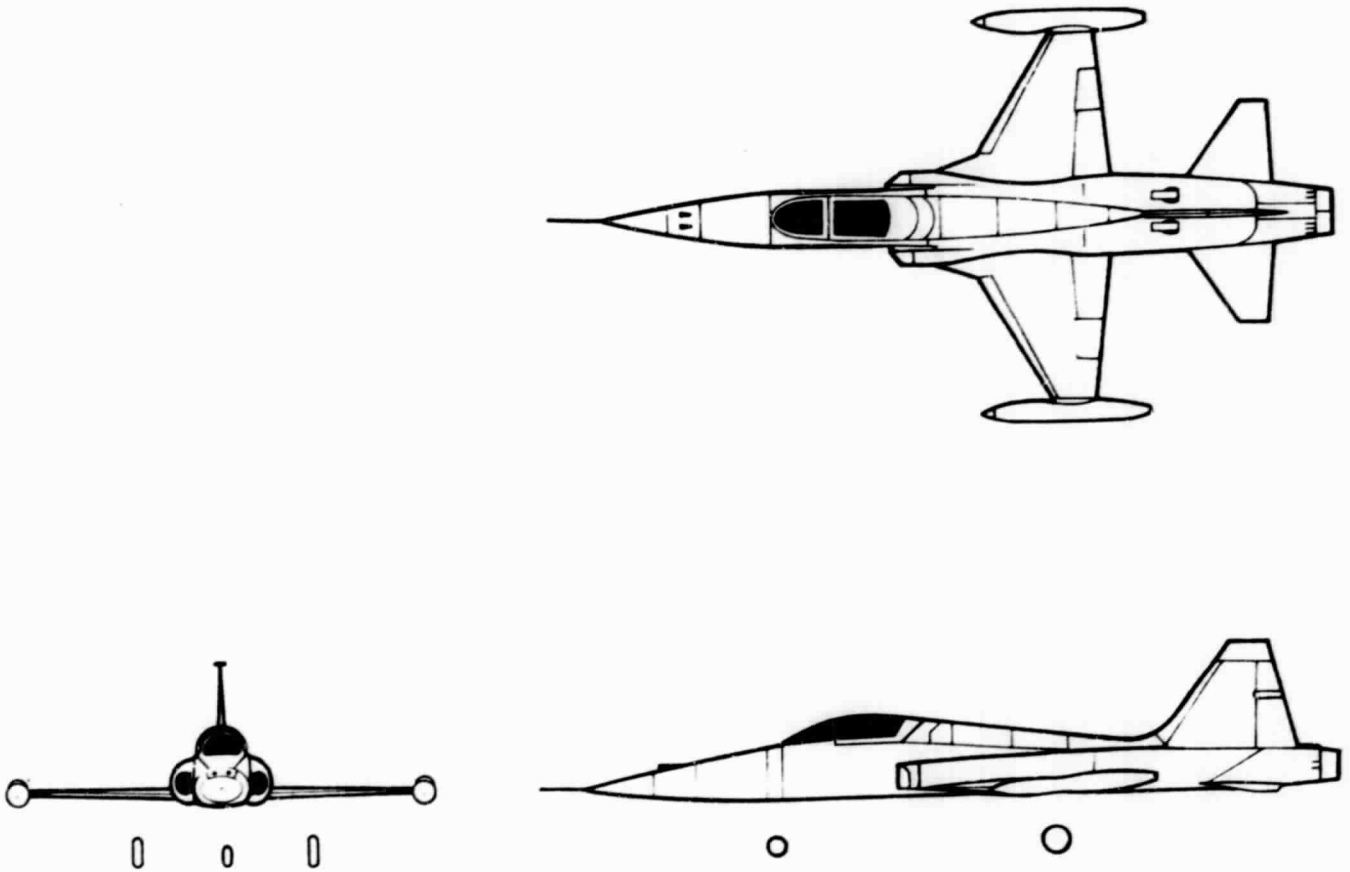

(a) Three-view.

Figure 18.- F-5.

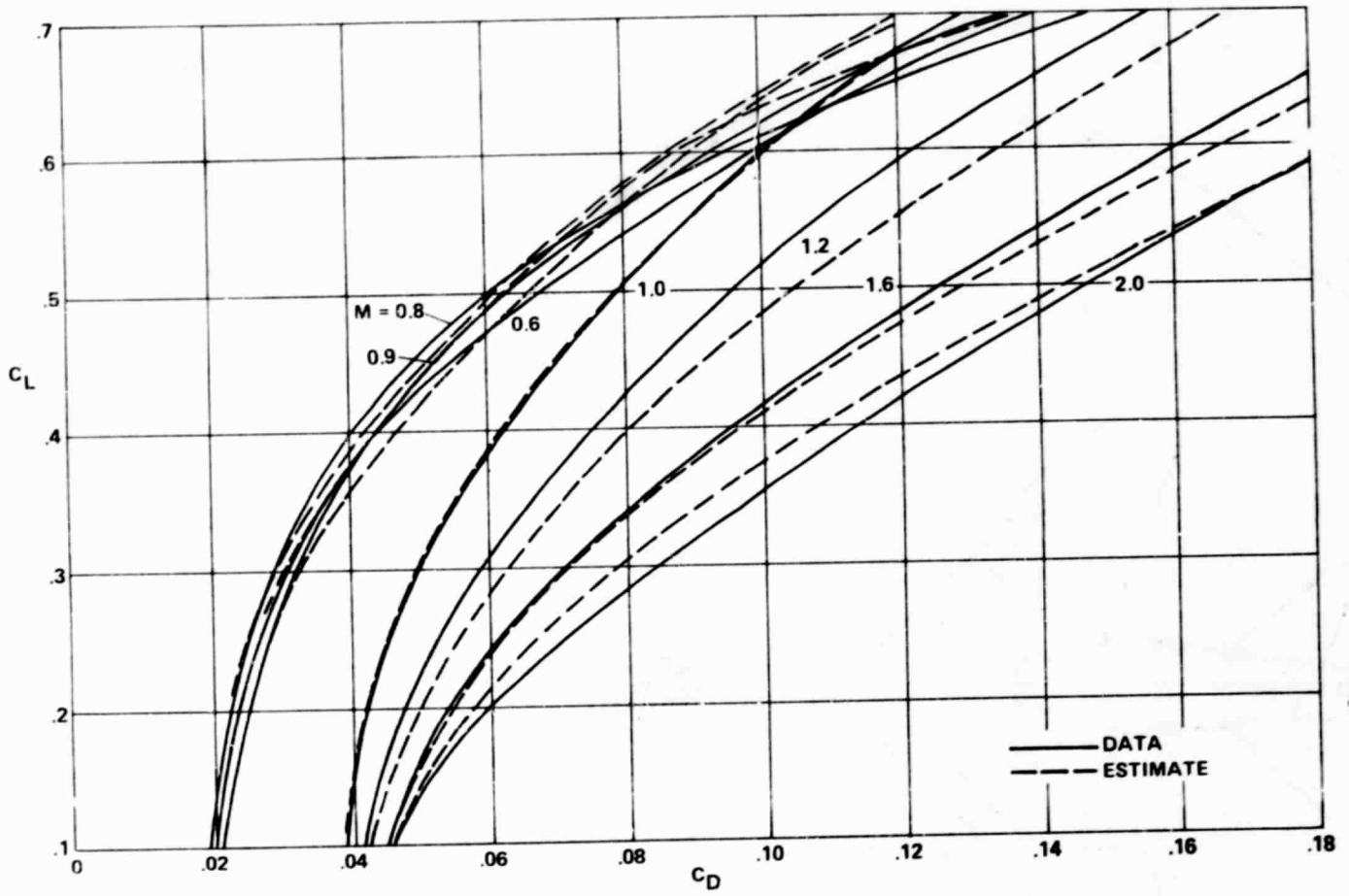

(b) Trimmed lift-drag polars.

Figure 18.- Concluded.

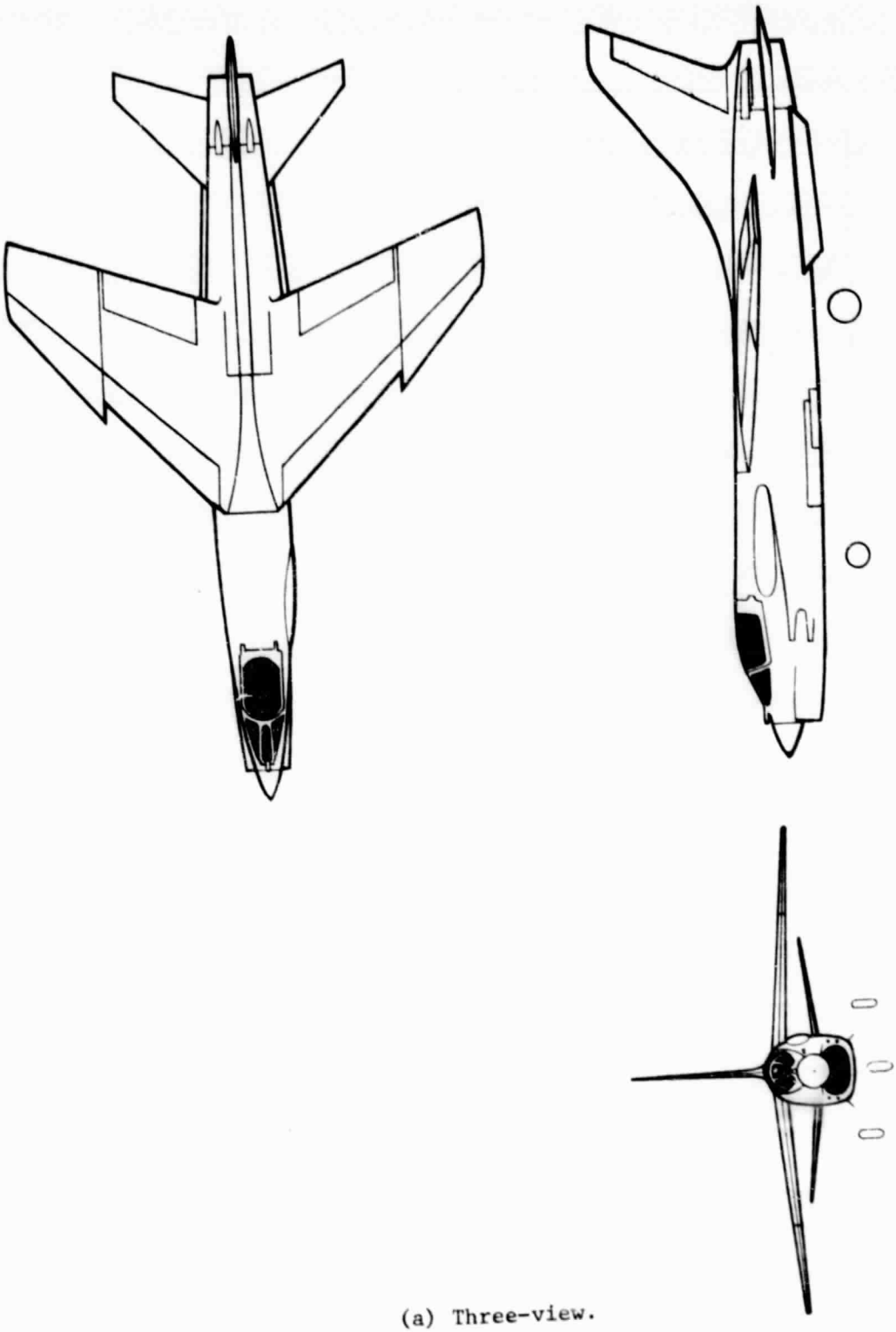

(a) Three-view.

Figure 19.- F-8.

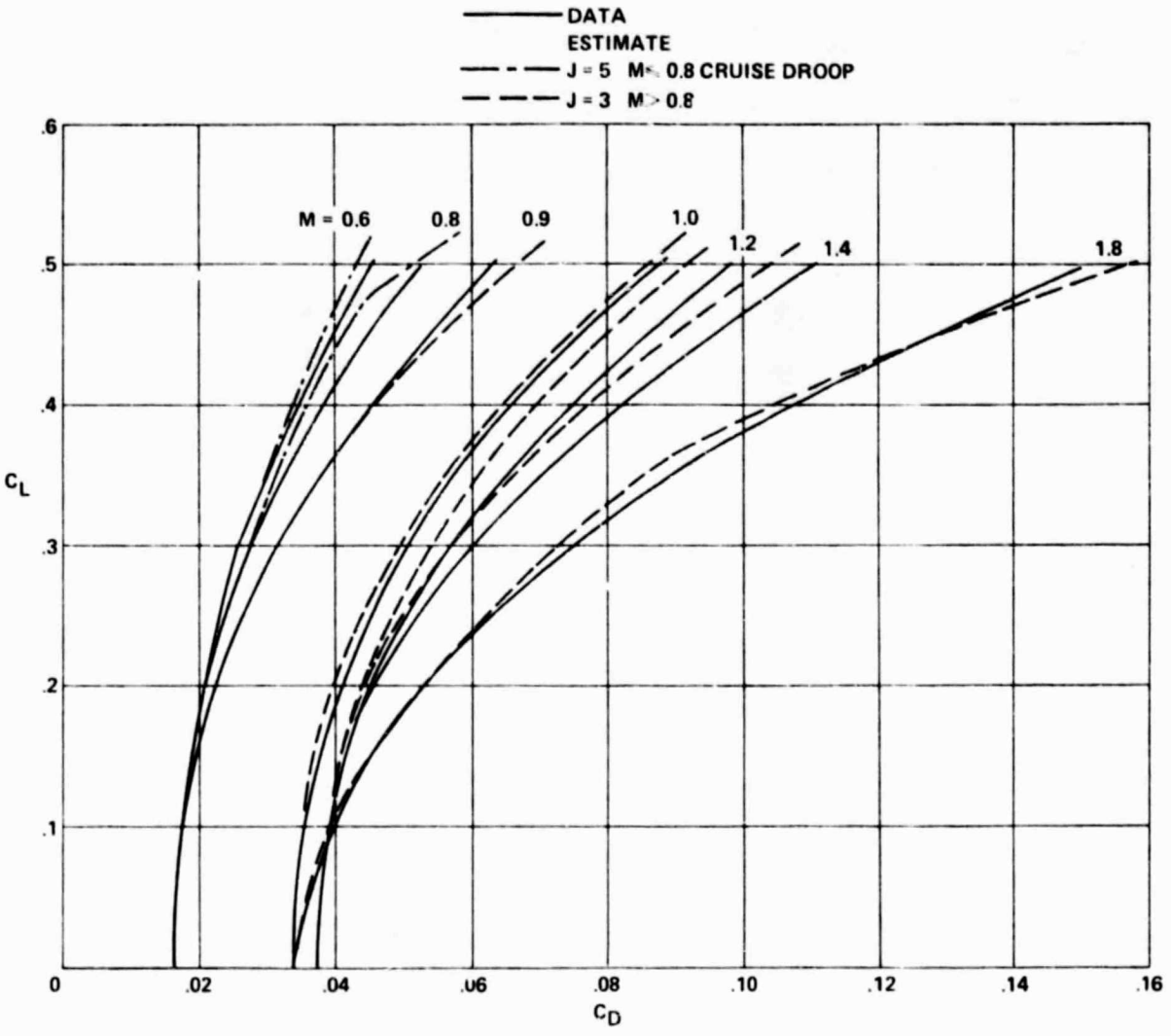

(b) Trimmed lift-drag polars.

Figure 19.- Concluded.

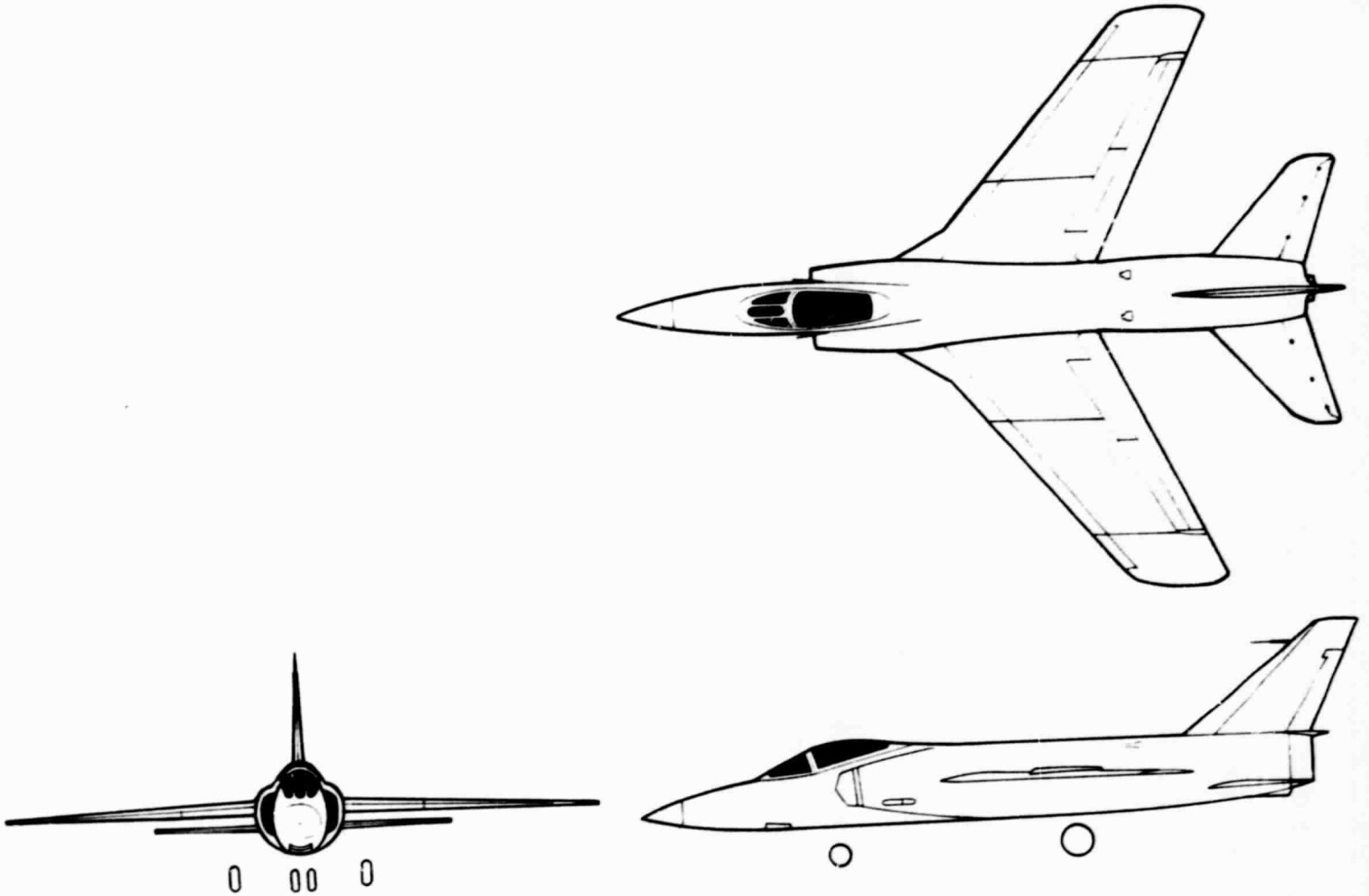

(a) Three-view.

Figure 20.- F-11.

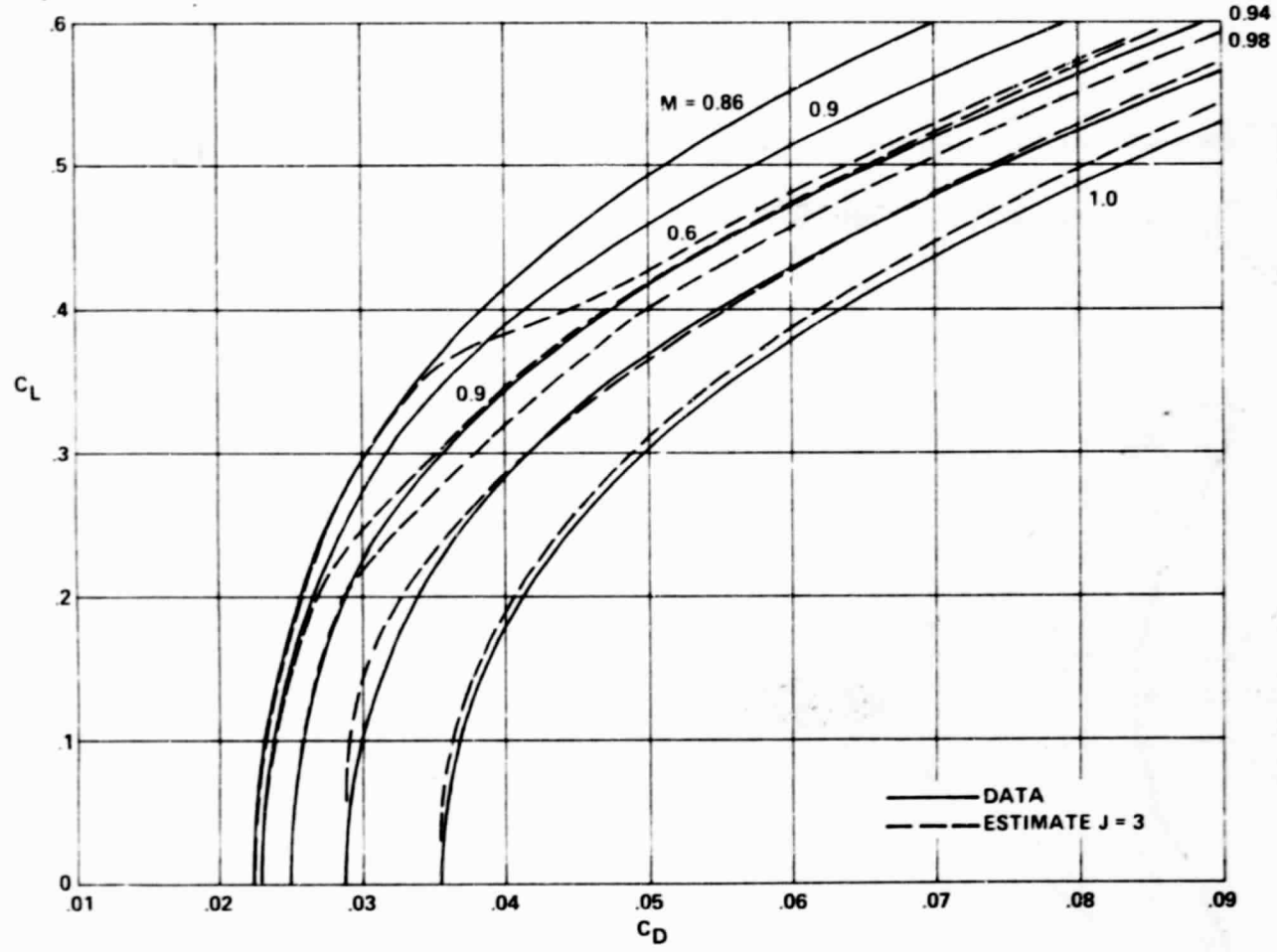

(b) Trimmed lift-drag polars.

Figure 20.- Concluded.

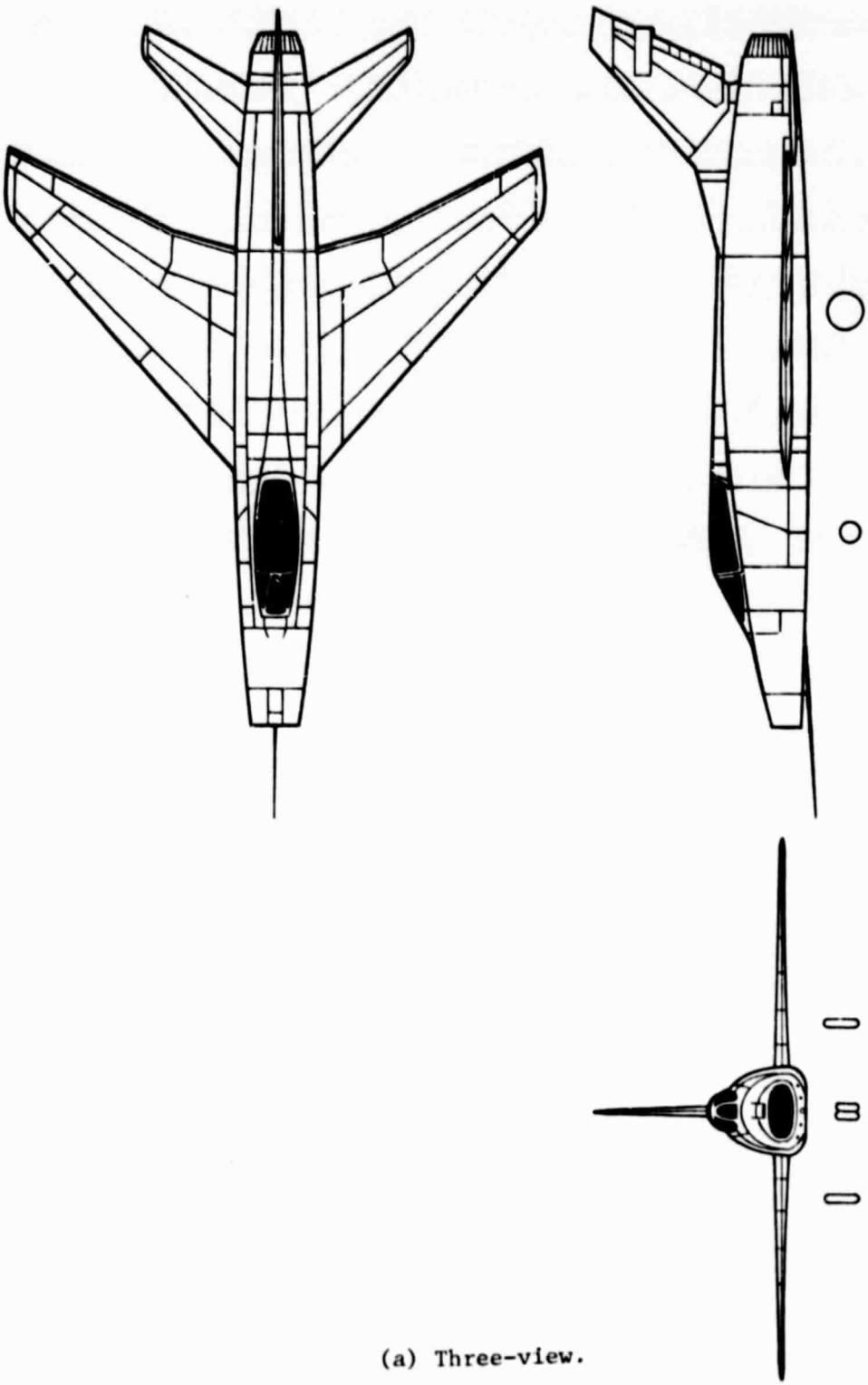

(a) Three-view.

Figure 21.- F-100.

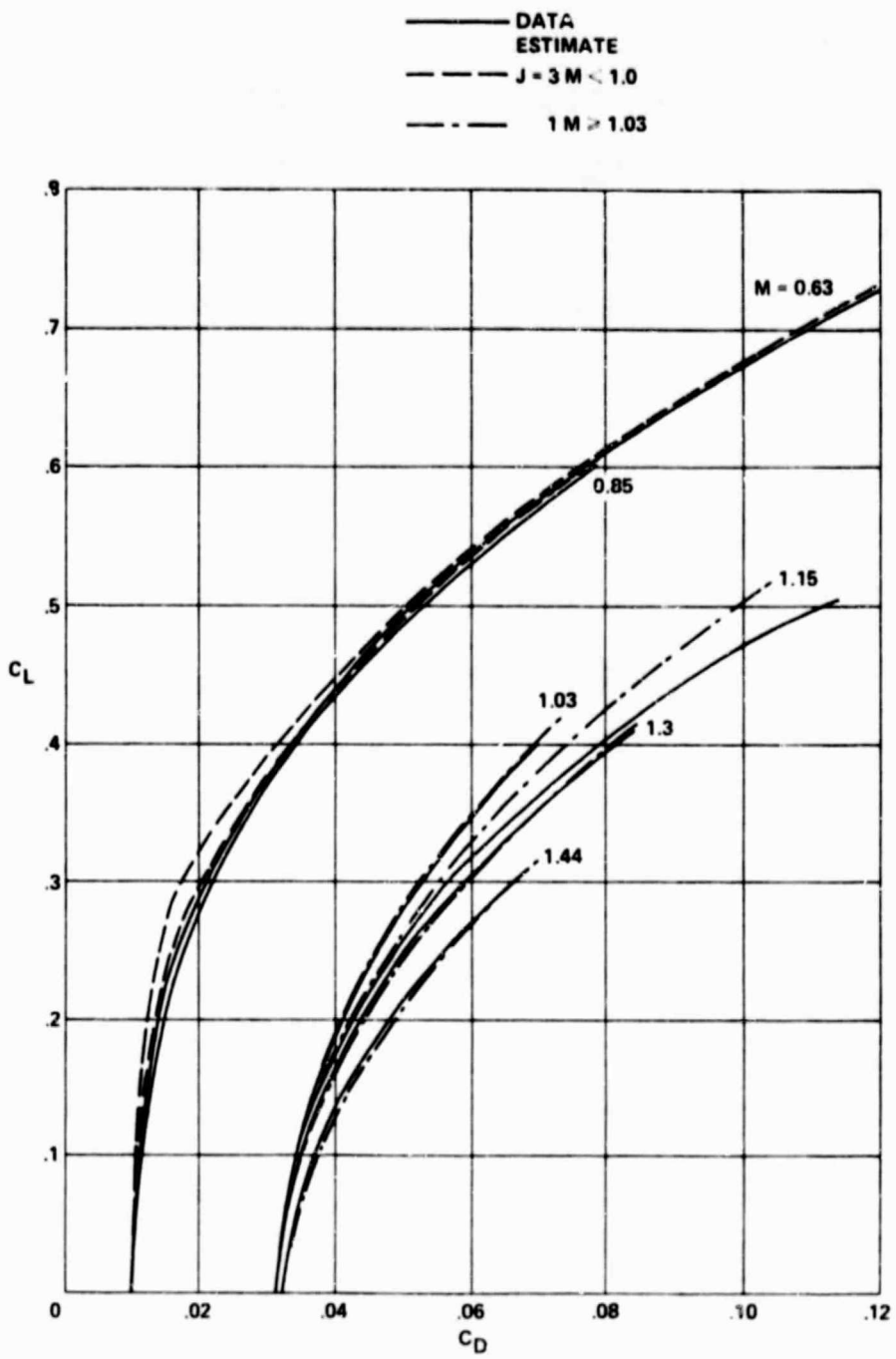

(b) Trimmed lift-drag polars.

Figure 21.- Concluded.

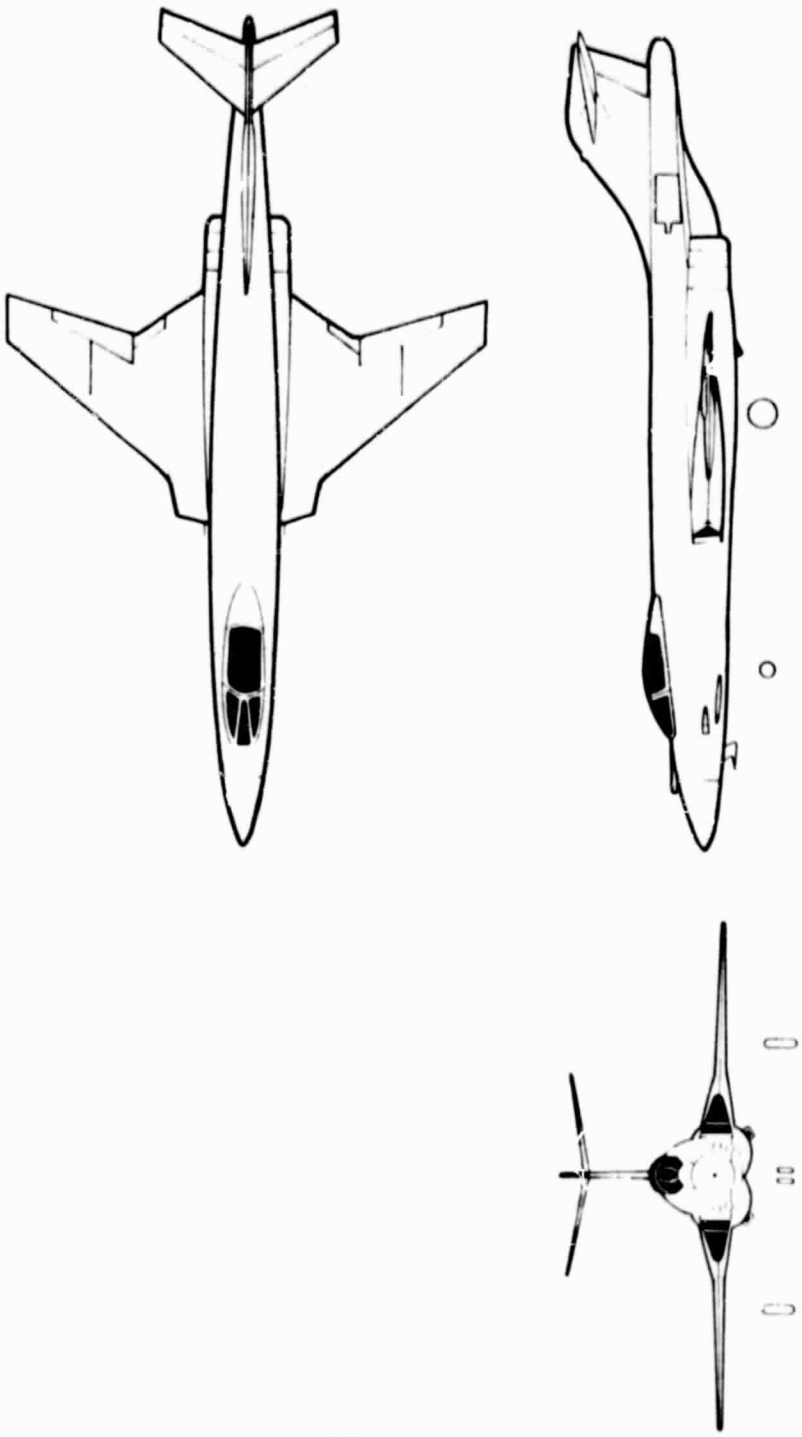

(a) Three-view.

Figure 22.- F-101.

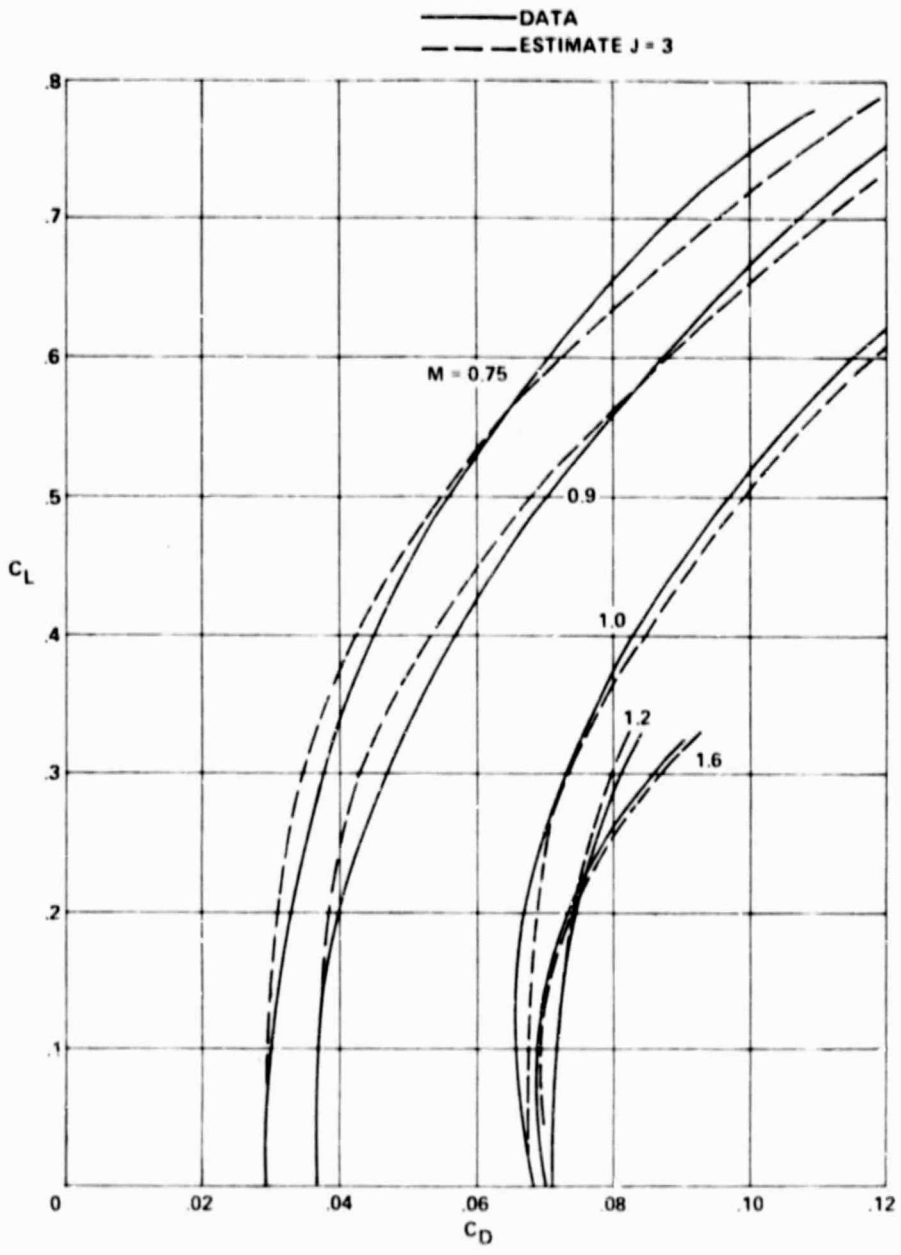

(b) Trimmed lift-drag polar.

Figure 22.- Concluded.

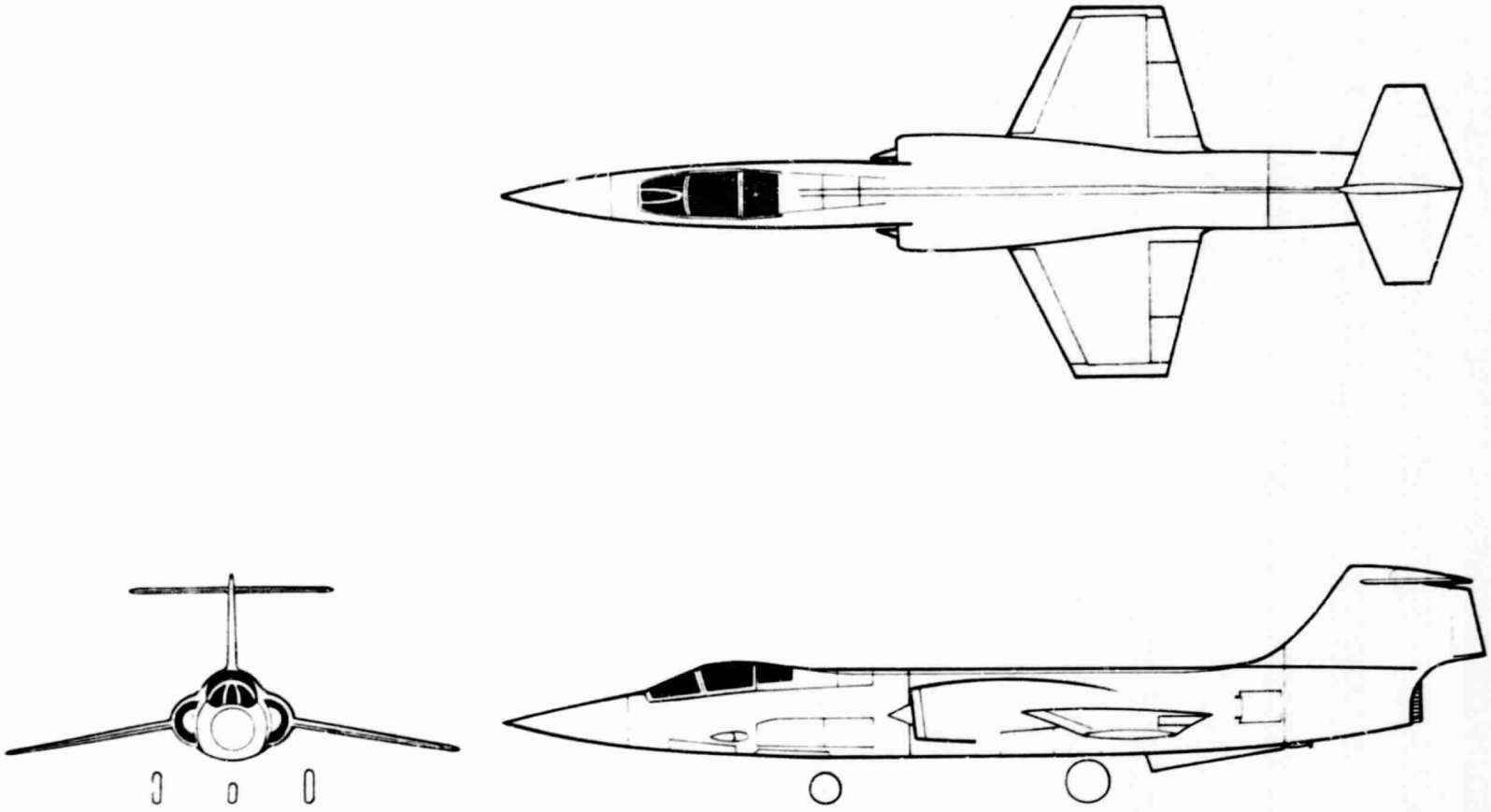

(a) Three-view.

Figure 23.- F-104.

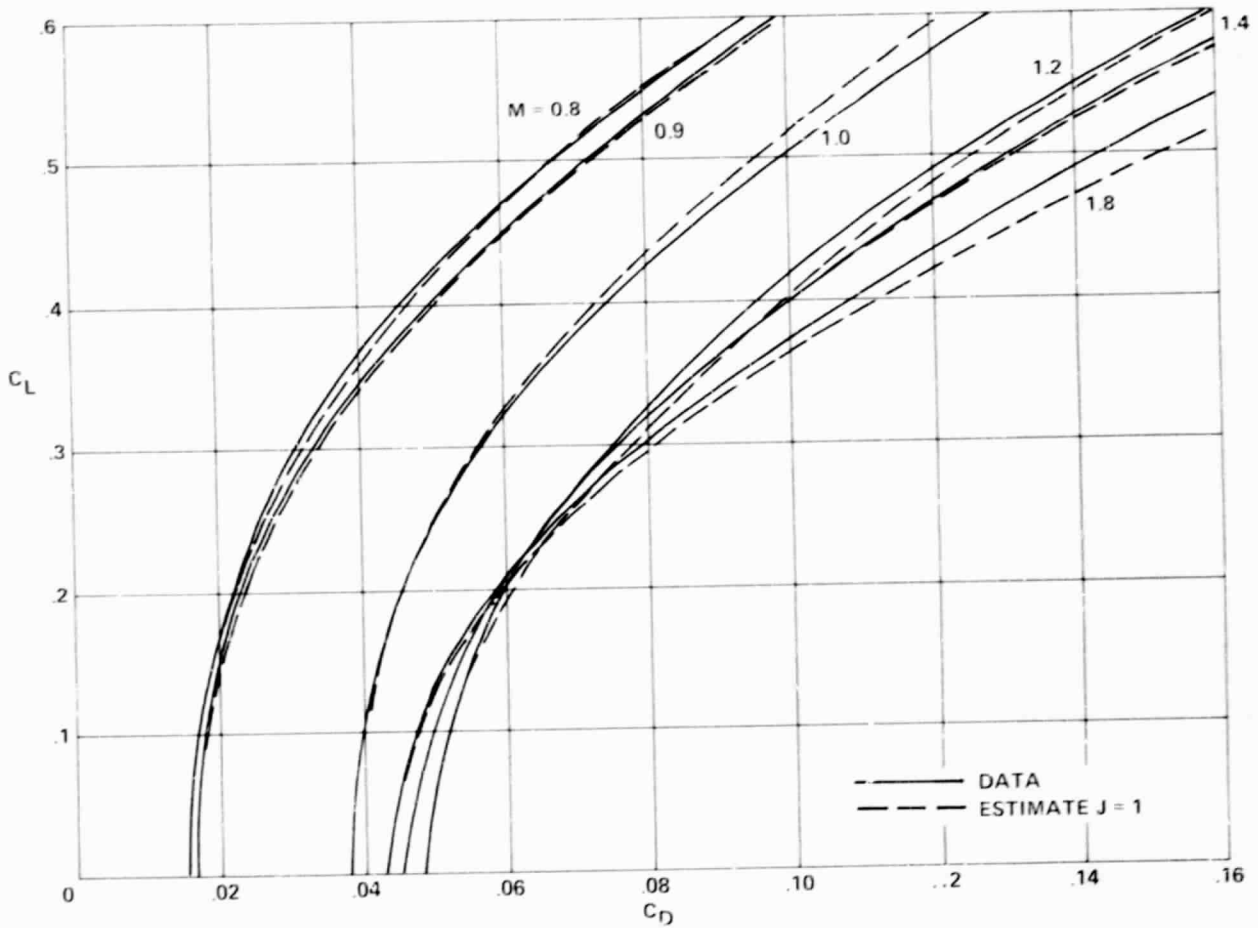

(b) Trimmed lift-drag polar.

Figure 23.- Concluded.

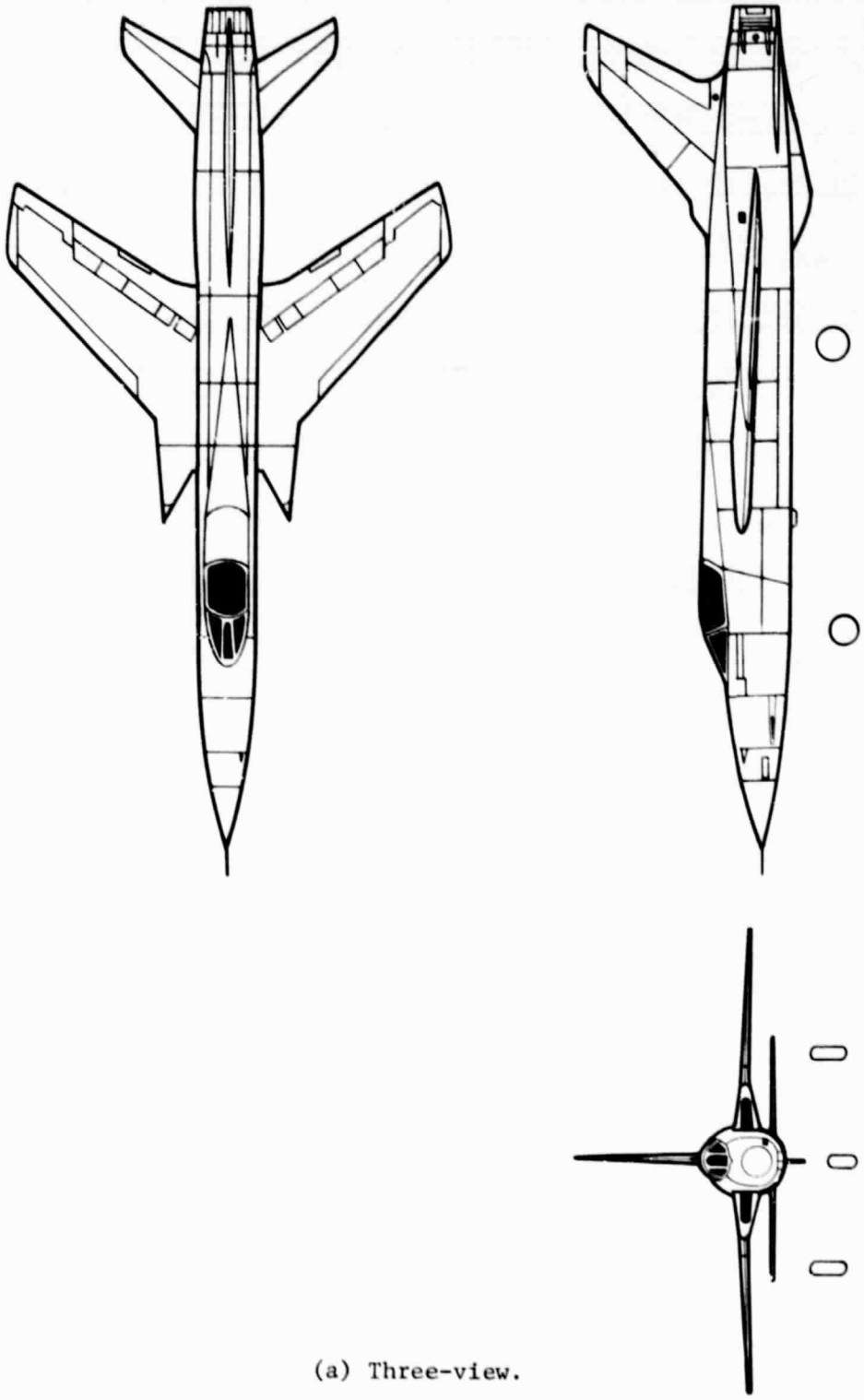

(a) Three-view.

Figure 24.- F-105.

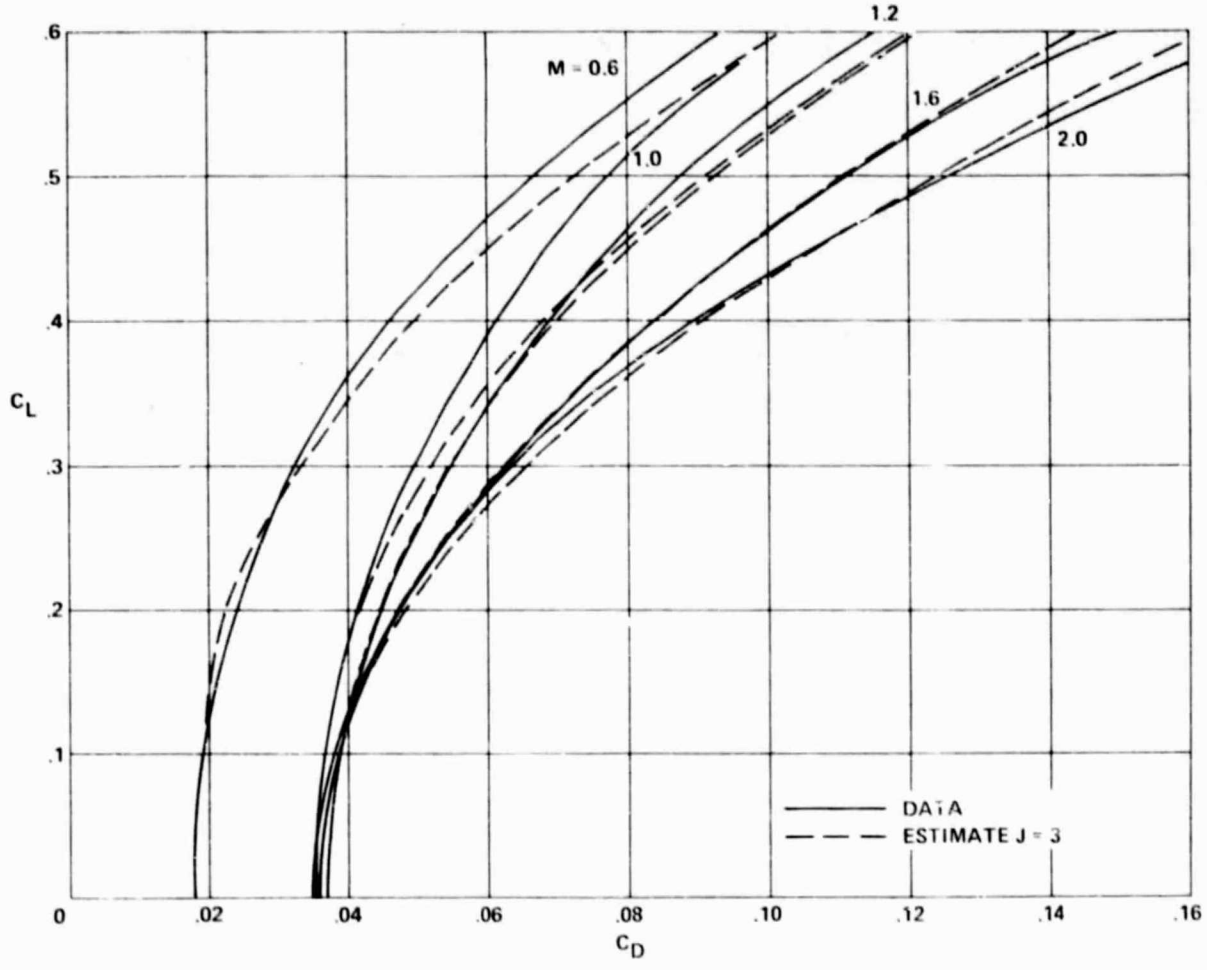

(b) Trimmed lift-drag polar.

Figure 24.- Concluded.

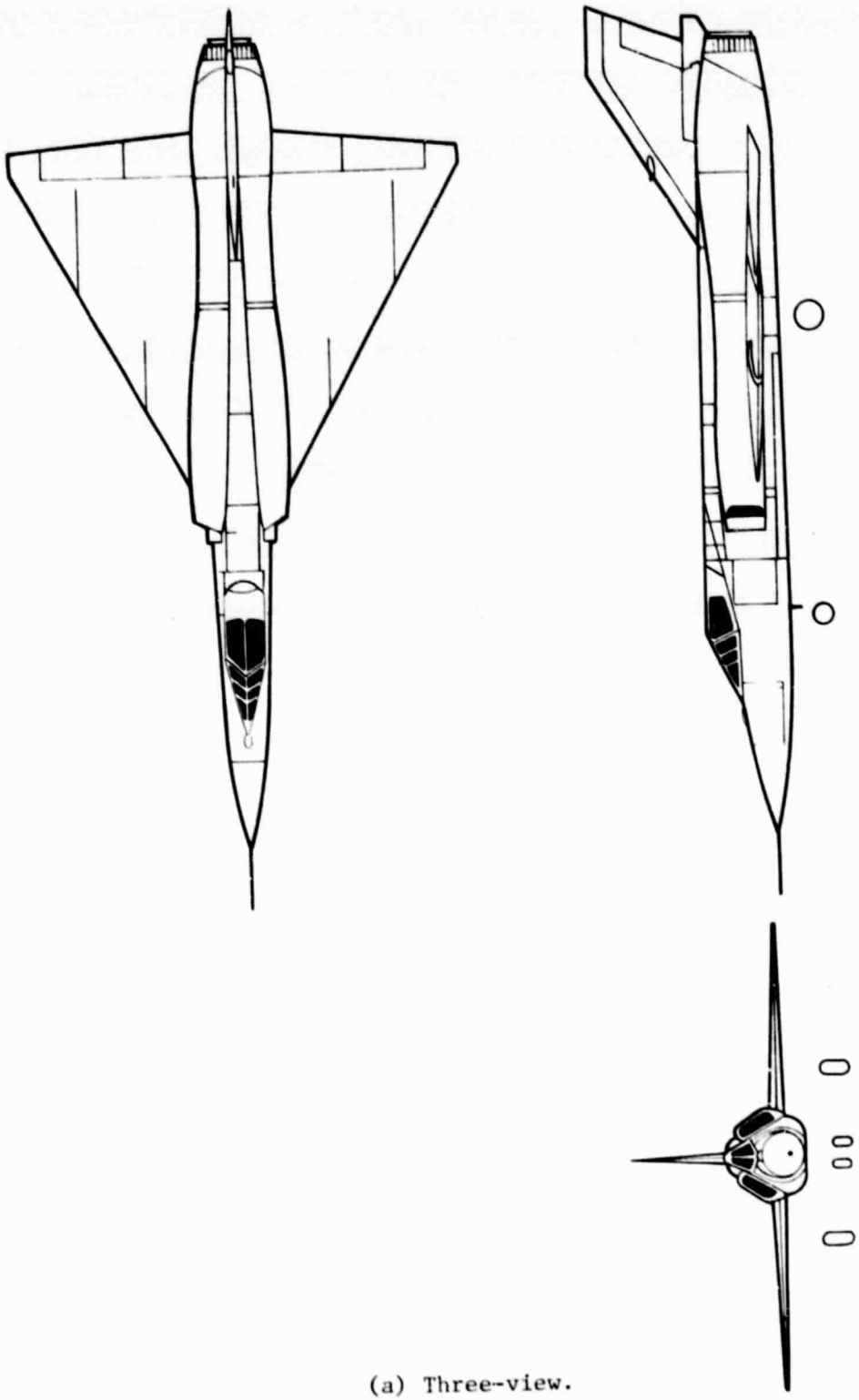

(a) Three-view.

Figure 25.- F-106.

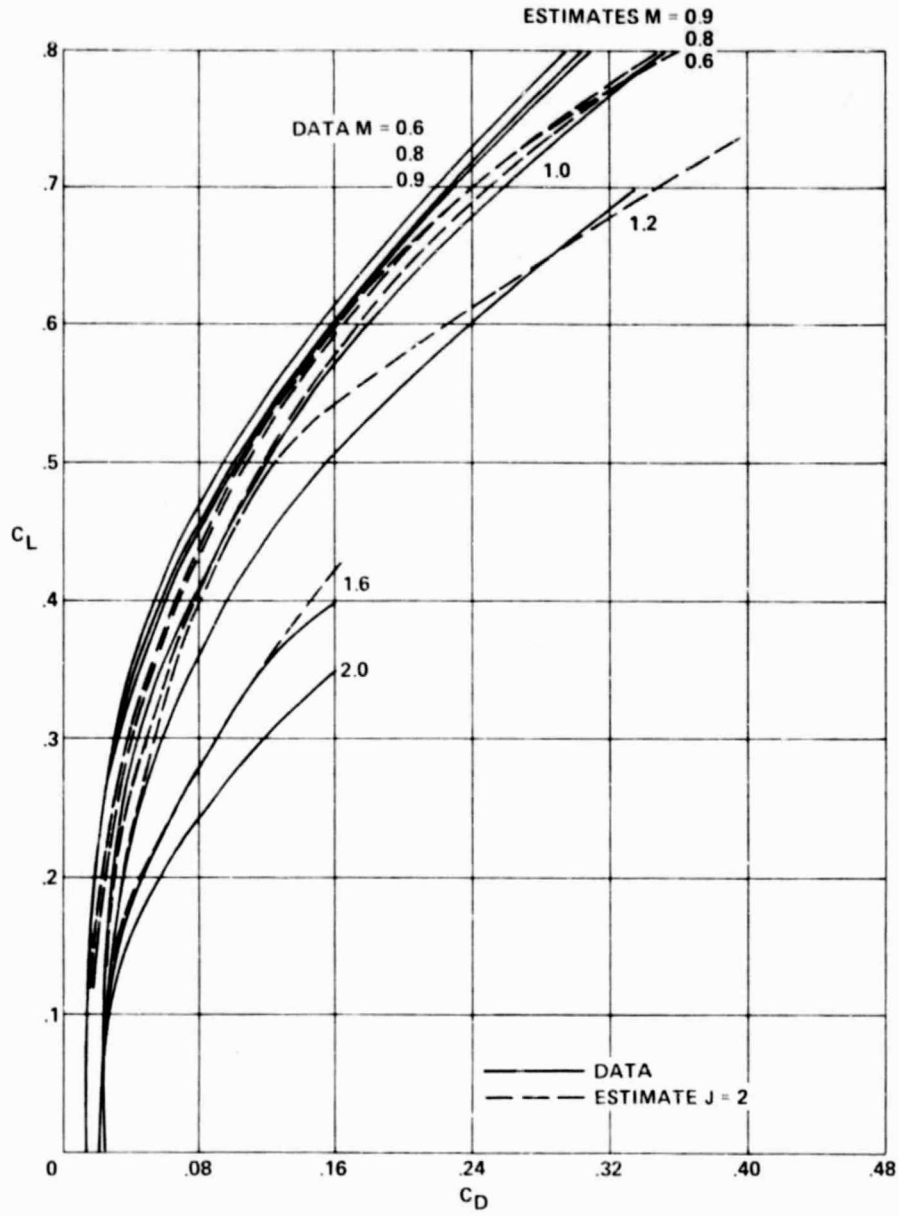

(b) Trimmed lift-drag polar.

Figure 25.- Concluded.

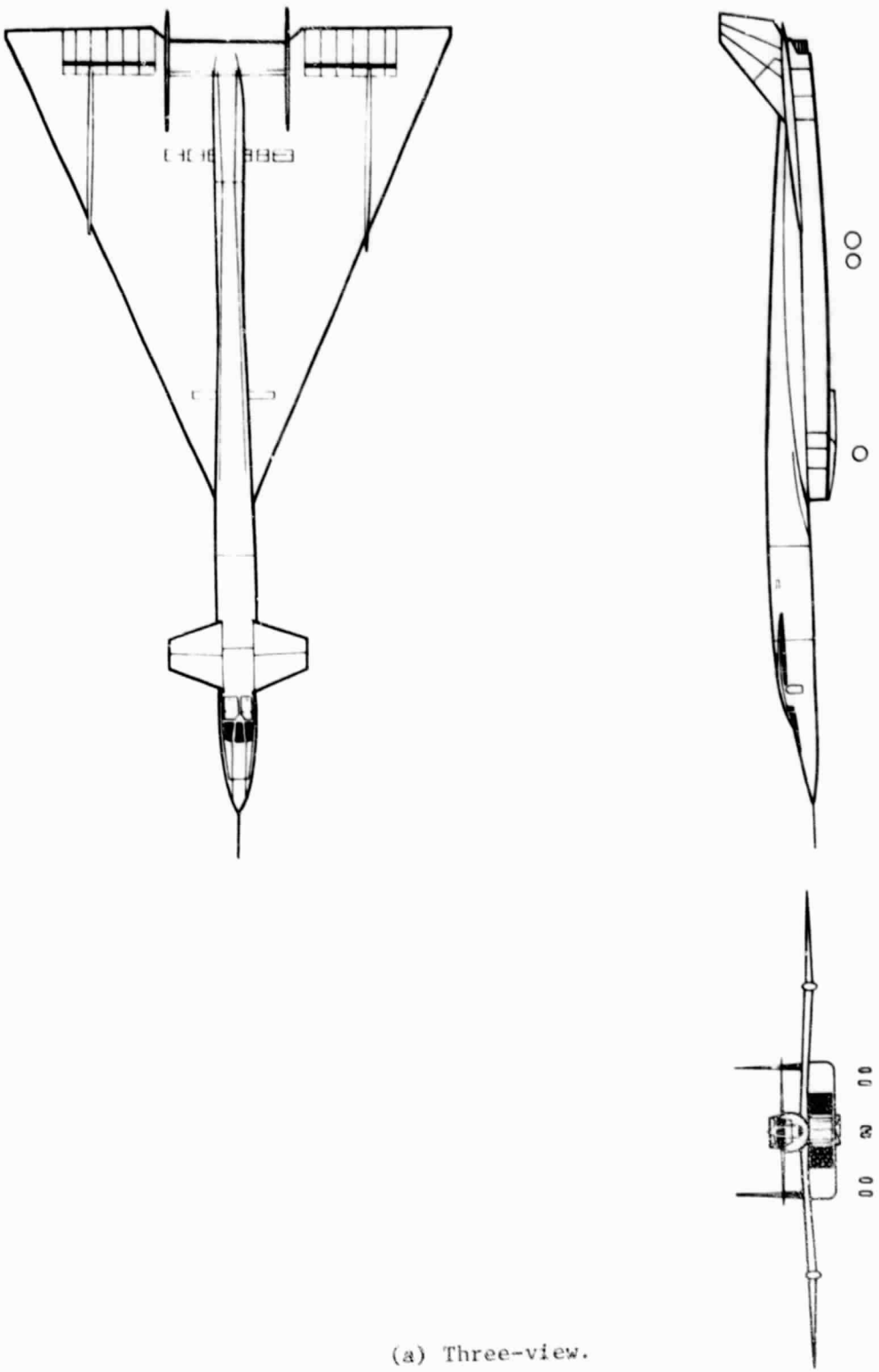

(a) Three-view.

Figure 26.- XB-70.

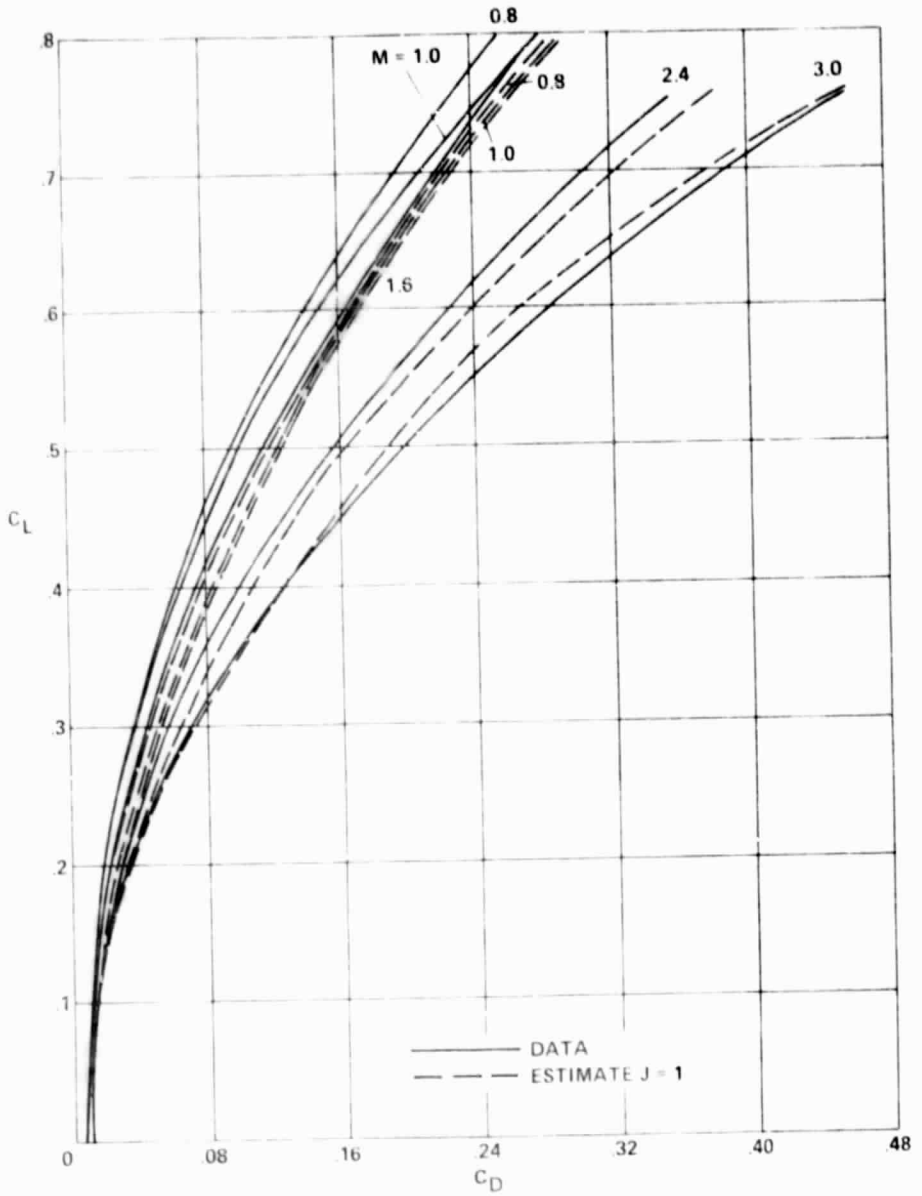

(b) Trimmed lift-drag polar.

Figure 26.- Concluded.